



Cite this: *Inorg. Chem. Front.*, 2022, 9, 5408

Recent advances in uranium-containing polyoxometalates

Guo-Ping Yang, a Ke Li *^a and Chang-Wen Hu *^b

Uranium-containing polyoxometalates (U-POMs), an important class of actinide cluster compounds, are the products of the assembly of uranium or uranium and POMs. These cluster compounds illustrate the structural beauty and diversity of obtained U-POMs that can be achieved by the reaction of uranium or uranium and POMs. The structural diversity is revealed by the classification of U-POMs in this review, which are mainly divided into two parts, according to the main metal elements of the clusters, named U-containing heteropolyoxometalates (U-hetero-POMs) and U-oxo-clusters. U-hetero-POMs are further classified by development date from the end of the 20th century based on the basic building units, including Keggin-type, Dawson-type, Silverton-type, hybrid structures, and cryptand structures. U-oxo-clusters mainly include uranyl peroxide clusters, their derivatives, and U^{IV}-oxo-clusters and mixed-valence U-oxo-clusters. This review provides a comprehensive summary of the synthesis and structures of U-POMs as well as their characterization, properties, and applications. Finally, the development prospects and directions for U-POMs in the future are also elucidated.

Received 24th August 2022,
Accepted 24th September 2022
DOI: 10.1039/d2qi01834a
rsc.li/frontiers-inorganic

^aJiangxi Province Key Laboratory of Synthetic Chemistry, Jiangxi Key Laboratory for Mass Spectrometry and Instrumentation, East China University of Technology, Nanchang, Jiangxi 330013, P. R. China. E-mail: like90@foxmail.com

^bKey Laboratory of Cluster Science of Ministry of Education, Beijing Key Laboratory of Photoelectronic/Electrophotonic Conversion Materials, School of Chemistry and Chemical Engineering, Beijing Institute of Technology, Beijing 100081, P. R. China. E-mail: cwhu@bit.edu.cn



Guo-Ping Yang

Dr Guo-Ping Yang received his B.S. degree from Changzhi University in 2011, his M.S. degree from Guangxi Normal University under the guidance of Prof. Feng Yang in 2014, and his Ph.D. degree from Beijing Institute of Technology in 2019 under the direction of Prof. Chang-Wen Hu. Then, he joined the Jiangxi Key Laboratory for Mass Spectrometry and Instrumentation of East China University of Technology. He focuses his research on exploring the synthesis, crystal structures, and properties of novel uranium-containing POMs, and the green catalytic organic synthesis of POMs.

1. Introduction

Polyoxometalates (POMs) are the most representative metal oxide clusters that self-assemble in solution with controllable structures and give us a unique way to design and synthesize metal oxide materials from the micro- to macro-scale. The incomparable chemical compatibility of POMs makes them ideal models to assess the influence of various elements on the structures and properties across the periodic table of



Ke Li

Dr Ke Li received his B.S. (2013), and Ph.D. degrees (2018) from Soochow University under the direction of Prof. Bao-Long Li. Then, he joined the Jiangxi Key Laboratory for Mass Spectrometry and Instrumentation and the School of Chemistry, Biology, and Materials Science in East China University of Technology. He currently works on crystalline functional materials including actinide-containing polyoxometal-organic frameworks, and

Dr Ke Li received his B.S. (2013), and Ph.D. degrees (2018) from Soochow University under the direction of Prof. Bao-Long Li. Then, he joined the Jiangxi Key Laboratory for Mass Spectrometry and Instrumentation and the School of Chemistry, Biology, and Materials Science in East China University of Technology. He currently works on crystalline functional materials including actinide-containing polyoxometal-organic frameworks, and

elements. Research on POMs has developed rapidly not only based on the fascinating structures but also the applications in various fields.^{1–8} One notes that the research trends of POMs have evolved from structure-driven research to performance-driven research in the past decades. In contrast, actinide-related POMs are less explored even if the first actinide-containing POMs were found more than 50 years ago.⁹ The studies of actinide-containing POMs may be limited by the difficulties in obtaining them and the radioactivity of actinides due to the strategic significance of actinides related to national defense, energy sources, and other fields, and the development of actinide-containing POMs lags far behind other transition metal (TM)-based POMs. But there are also several investigations on actinide-containing POMs, involving Th, U, Np, Pu, and Am.^{10–17} However, only U-related POMs are studied relatively more due to the stability of isotopes and the difficulty in acquiring the actinides.

Uranium is one of the most important strategic resources in the nuclear industry and exhibits abundant oxidation states from +2 to +6.^{18,19} Uranium chemistry already developed into the representative field of actinide chemistry.^{20–23} The most stable state of +6 uranium atoms is to form linear uranyl ions (UO_2^{2+}) combining two oxygen atoms with triple bonds. However, the two opposite oxygen atoms are inert under the most common conditions. One uranyl ion could coordinate with at most six oxygen atoms in a hexagonal bipyramidal geometry.²⁴ While, 5-coordinated uranyl in pentagonal bipyramidal geometry is more commonly found. Uranium atoms with a +4 oxidation state exhibit different coordination behaviors, which are more similar to other tetravalent transition metal ions such as Zr^{4+} and Hf^{4+} .^{25–28} Tetravalent uranium also shows more abundant coordination modes and the coordination numbers could be 12 or higher.⁹ Thus, the combination of uranium atoms and traditional POMs has a strong coordi-

nation basis. Besides, the polymerizable nature of uranyl ions and tetravalent uranium salts in aqueous solutions makes them easy to assemble into U-oxo-clusters, clusters built from a certain number of UO_2^{2+} or U^{4+} ions and bridging oxygen linkers, which is also a significant category of POM chemistry.^{10,18} One can see the trend that the research focus of U-containing POMs (U-POMs) has gradually turned into structure-based performance research not only due to the development tendency of chemistry but also the increasing numbers of new U-POMs prepared in recent years.

To better summarize the structural features, the U-POMs in this review are mainly divided into two parts, U-containing heteropolyoxometalates (U-hetero-POMs) and U-oxo-clusters. U-hetero-POMs are those POMs in which the early transition metal elements (W etc.) are the main part of the clusters and uranium is the heterometal ion. While U-oxo-clusters are those POMs in which uranium atoms are the main building units of clusters. Thus, the U-POMs discussed in this review are divided into three parts: (i) U-hetero-POMs, which are classified based on the building units, including Keggin, Dawson, Silverton, and so on; (ii) U-oxo-clusters reported in recent years, including uranyl peroxide clusters, POM-related uranium phosphates derivatives, U-oxo-clusters containing other transition metals, and U^{IV} -oxo-clusters and mixed-valence U-oxo-clusters; (iii) other types of U-POMs, which are hard to classify. This review restricts our attention to U-hetero-POMs and recent U-oxo-clusters containing four or more essential uranium atoms. We focus on the development of U-POMs with respect to the aspects of syntheses, structures, properties, and applications. Finally, several directions for further research are proposed.

2. Synthesis and structure of U-POMs

2.1 U-hetero-POMs

U-hetero-POMs are built from traditional POM building units with different kinds of lacunary precursors or from simple starting materials (such as Na_2WO_4 , heteroatom salts, etc.). $\text{UO}_2(\text{NO}_3)_2$ and $\text{UO}_2(\text{OAc})_2$ (OAc = acetate) are the most commonly used uranium sources and the employment of UCl_4 or $\text{U}(\text{SO}_4)_2$ may introduce considerable uncertainty for the synthesis of novel U-hetero-POMs due to the oxidation and richer bonding ability of U^{IV} . Those U-hetero-POMs based on Keggin-type lacunary precursors are the most reported due to the natural stability of Keggin-type lacunary precursors. Consequently, the U-hetero-POMs here are divided up based on the basic building blocks, including Keggin-type, Dawson-type, Silverton-type, hybrid structures, and cryptand structures (Table 1).

2.1.1 Keggin-type structures. It is known that Keggin-POMs are the first and the most widespread kind of POMs to be studied. Stable Keggin-type lacunary precursors and Keggin-POM derivatives are also the most abundant. In most cases, polyvacant polyoxotungstates (POWs) are the most stable, and



Chang-Wen Hu

Prof. Chang-Wen Hu received his Ph.D. from the University of Tokyo in 1993 and worked as a JSPS visiting professor at the Tokyo Institute of Technology and National Institute of Advanced Science and Technology (AIST), Japan before joining the Beijing Institute of Technology in 2002. He received the MOE Natural Science Award (First Prize) in 2012 and the MOE Technological Progress Award (Third Prize) in 1999. He

has authored or co-authored over 200 peer-reviewed papers and was honored as one of the most cited Chinese researchers of 2015 (Thomson Reuters). His research interests involve energy storage and conversion, multifunctional nanomaterials, polyoxometalate chemistry, and CO_2 chemistry.

Table 1 Summary of U-hetero-POMs with crystal structures

Table 1 (Contd.)

Type	Compounds	Building Units	Materials of POMs	Reaction Temp./°C	pH	Ref.
Cryptand	$(\text{NH}_4)_{11}[\text{U}(\text{H}_2\text{O})\text{P}_5\text{W}_{30}\text{O}_{110}] \cdot 12\text{H}_2\text{O}$	$\{\text{P}_5\text{W}_{30}\}$	$\{\text{P}_5\text{W}_{30}\}$	60–70/ 140–180	—	63
	$[(\text{UO}_2)_3(\text{H}_2\text{O})_6\text{As}_3\text{W}_{30}\text{O}_{105}]^{15-}$	$\{\text{As}^{\text{III}}\text{W}_9\}_3(\text{W}_3)$	$\{\text{As}^{\text{III}}\text{W}_9\}_3(\text{W}_3)$	90	$5.4/3.8 \pm 0.2$	60
	$(\text{NH}_4)_7[(\text{UO}_2)_3(\text{H}_2\text{O})_6\text{As}_3\text{W}_{29}\text{V}^{\text{IV}}\text{O}_{105}] \cdot 4\text{H}_2\text{O}$	$\{\text{As}^{\text{III}}\text{W}_9\}_2(\text{V}^{\text{IV}}\text{W}_2)$	$[(\text{UO}_2)_3(\text{H}_2\text{O})_5\text{As}_3\text{W}_{29}\text{O}_{104}]^{19-}$ and VOSO ₄	r.t.	—	34
	$[\text{Na}(\text{UO}_2)_3(\text{OH})(\text{H}_2\text{O})_6\text{As}_4\text{W}_{40}\text{O}_{140}(\text{WO})]^{18-}$	$\{\text{As}^{\text{III}}\text{W}_{40}\}$	$\{\text{As}^{\text{III}}\text{W}_{40}\}$	r.t.	—	64
	$[\text{U}_2^{\text{IV}}(\mu_2\text{-OH})_3(\mu_2\text{-O})]\text{As}_4\text{W}_{40}\text{O}_{140}]^{25-}$	$\{\text{As}^{\text{III}}\text{W}_{40}\}$	$\{\text{As}^{\text{III}}\text{W}_{40}\}$	70	4.7	4.7
	$[\text{U}_2^{\text{IV}}(\mu_2\text{-O})_3(\text{HCOO})_3]\text{As}_4\text{W}_{40}\text{O}_{140}]^{20-}$	$\{\text{As}^{\text{III}}\text{W}_{40}\}$	$\{\text{As}^{\text{III}}\text{W}_{40}\}$	70	4.7	4.7
	$[\text{U}_4^{\text{IV}}(\mu_2\text{-O})_2(\text{HCOO})_4]\text{As}_4\text{W}_{40}\text{O}_{140}]^{20-}$	$\{\text{As}^{\text{III}}\text{W}_{40}\}$	$\{\text{As}^{\text{III}}\text{W}_{40}\}$	160	3.7	4.8
	$[(\text{UO}_2)_{7.2}(\text{HCOO})_{7.8}(\text{P}_8\text{W}_{48}\text{O}_{184})\text{Cl}_8]^{41.4-}$	$\{\text{P}_8\text{W}_{48}\}$	$\{\text{P}_8\text{W}_{48}\}$	Reflux	6.2 or 6.6/1.5	49
	$[(\text{UO}_2)_8(\text{P}_8\text{W}_{48}\text{O}_{184})]^{24-}$	$\{\text{P}_8\text{W}_{48}\}$	$\{\text{P}_8\text{W}_{48}\}$	50	6.2 or 6.6/1.5	50
	$\{[(\text{UO}_2)_4(\text{O}_2)_2(\text{P}_8\text{W}_{48}\text{O}_{184})]^{40-}$	$\{\text{P}_8\text{W}_{48}\}$	$\{\text{P}_8\text{W}_{48}\}$	6.0/5.7	6.0/5.7	50

Temperatures not mentioned in the original text are room temperature (r.t.) by default except for the unverifiable Silverton structures.

the basic mono-, bi-, and trivacant Keggin-type precursors $\{\text{XW}_{11}\}$, $\{\text{XW}_{10}\}$, $\{\text{XW}_9\}$ tolerate various heteroatoms including B, Si, Ge, P, As, Sb, Bi, S, Se, Te, etc. Thus, Keggin-type U-hetero-POWs are also the most studied. The first Keggin-type U-hetero-POW for which a single-crystal structure was recorded might be monovacant $\{\text{GeW}_{11}\}$ -based $\text{Cs}_{12}[\text{U}(\text{GeW}_{11}\text{O}_{39})] \cdot 13\text{–}14\text{H}_2\text{O}$ reported by Tourné and co-workers in 1980 (Fig. 1a).²⁹ Most of the Keggin-type U-hetero-POMs based on trivacant precursors show similar sandwich structures in which two trivacant $\{\text{XW}_9\}$ sandwich a tri- or tetrานuclear cluster containing 2 to 4 UO_2^{2+} or U^{4+} . The empty position in the sandwich was occupied by H_2O or counter cations such as Na^+ , K^+ , and NH_4^+ (Fig. 1b and c). Pope synthesized the first series of typical sandwich-type U-hetero-POWs with the general formula of $[\text{M}_2(\text{UO}_2)_2(\text{PW}_9\text{O}_{34})_2]^{12-}$ ($\text{M} = \text{Na, K, NH}_4$) in 1999 (Fig. 1b and c).³⁰ $[\text{Na}_2(\text{UO}_2)_2(\text{PW}_9\text{O}_{34})_2]^{12-}$ represented the first typical sandwich structure, in which two $\{\text{PW}_9\}$ sandwiched a $\{\text{Na}_2(\text{UO}_2)_2\}$ cluster to form the symmetrical U-hetero-POWs (Fig. 1b). $[\text{K}_2(\text{UO}_2)_2(\text{PW}_9\text{O}_{34})_2]^{12-}$ and $[(\text{NH}_4)_2(\text{UO}_2)_2(\text{PW}_9\text{O}_{34})_2]^{12-}$ showed another typical asymmetric sandwich structure in which two uranyl ions and K^+ or NH_4^+ were sandwiched with a triangular configuration (Fig. 1c). Recently, our group also synthesized five $\{\text{Na}_2(\text{UO}_2)_2(\text{XW}_9\text{O}_{34})_2\}$ -based ($\text{X} = \text{P/Si}$) U-POMs with different 2D/3D structures, which revealed the significant influence of counter cations on the spatial structures of U-POMs even if the structures of $\{\text{Na}_2(\text{UO}_2)_2(\text{XW}_9\text{O}_{34})_2\}$ were similar.^{31–33} Our work demonstrates that different reaction conditions provide the assembly conditions for Na- H_2O clusters with different coordination environments and different dimensions, which result in different spatial structures.

Rusu studied the properties of four Keggin-type compounds, including isotope exchange, spectroscopy, thermal analyses, magnetic susceptibility, and paper electrophoresis in 1999 and 2000.^{65–67} However, only the formulas, i.e., $\text{Na}_{12}[(\text{UO})_3(\text{H}_2\text{O})_6(\text{PW}_9\text{O}_{34})_2] \cdot 21\text{H}_2\text{O}$, $\text{K}_{12}[\text{U}^{\text{IV}}(\text{BW}_{11}\text{O}_{39}\text{H})_2] \cdot 23\text{H}_2\text{O}$, $\text{K}_4[\text{U}^{\text{IV}}\text{GeW}_{11}\text{O}_{39}]$, and $\text{K}_{12}[\text{U}^{\text{IV}}(\text{GeW}_{11}\text{O}_{39})_2]$, were provided without crystal data. Then, David prepared two sandwich-type structures with formulas of $\text{Na}_{14}[(\text{U}^{\text{IV}}\text{O})_3(\text{GeW}_9\text{O}_{34})] \cdot 23\text{H}_2\text{O}$ and $\text{Na}_6[\text{U}_3^{\text{IV}}(\text{SbW}_9\text{O}_{33})_2] \cdot 22\text{H}_2\text{O}$, but crystal data were also not provided.^{68,69} The utilization of $\text{U}(\text{SO}_4)_2$, prepared from $\text{UO}_2(\text{OAc})_2$ hydrate, should be a key factor for the formation of these U^{IV} -hetero-POWs.

Compared with trivacant precursors, there are much fewer Keggin-type bivacant precursors. As a result, there were only two cases based on $\{\gamma\text{-SiW}_{10}\}$, which were also reported by Pope in 2002.³⁴ In this work, Pope reported five Keggin-derivative U-hetero-POWs, among which $[\text{Na}_2(\text{UO}_2)_2(\text{SiW}_9\text{O}_{34})_2]^{14-}$ showed a typical sandwich structure based on trivacant $\{\text{SiW}_9\}$ (Fig. 1b). Another two tetramers $[(\text{M}(\text{OH}_2))_4(\text{UO}_2)_4(\text{OH})_2(\text{SiW}_{10}\text{O}_{36})_4]^{22-}$, $\text{M} = \text{Na/K}$, are the only two bivacant precursor-based structures (Fig. 1k and l). The arrangement of four uranyl ions in the two tetrameric structures was similar to the $\{\text{As}_4\text{W}_{40}\}$ -based structures reported by Duval in 2018 (section 2.1.5).⁶⁴ However, it could be found that Na^+ and K^+ in the two structures displayed different arrangements. Na^+ ions are adja-

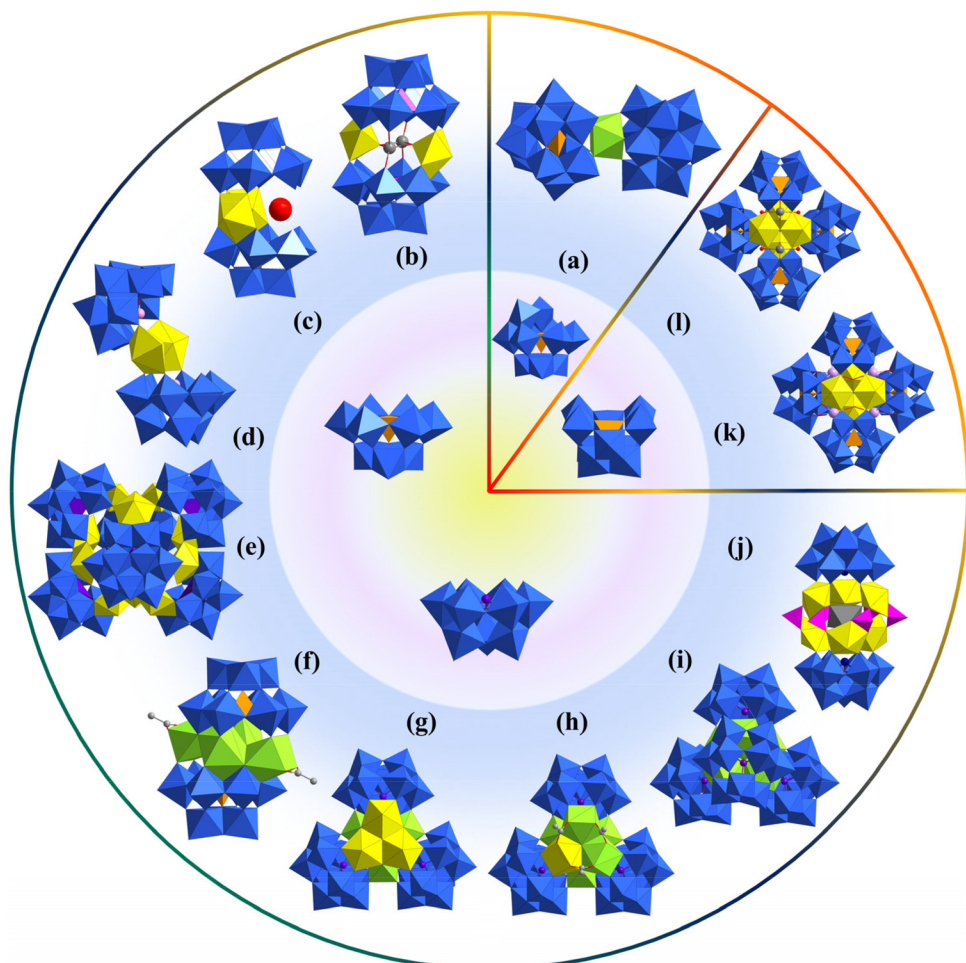


Fig. 1 View of Keggin-type U-hetero-POWs. (a) $[\text{U}(\text{GeW}_{11}\text{O}_{39})_2]^{12-}$; typical structures of (b) $\{\text{Na}_2(\text{UO}_2)_2(\text{XW}_9\text{O}_{34})_2\}$ ($\text{X} = \text{Si, P, Ge, As}^{\text{V}}$), (c) $\{\text{M}_2(\text{UO}_2)_2(\text{XW}_9\text{O}_{34})_2\}$ ($\text{M} = \text{H}_2\text{O, NH}_4^+, \text{K}^+; \text{X} = \text{Si, P, As}^{\text{V}}$), (d) the “open” sandwich structure of $\{(\text{UO}_2)_2(\text{H}_2\text{O})_2(\text{XW}_9\text{O}_{33})_2\}$ ($\text{X} = \text{As}^{\text{VI}}, \text{Sb}^{\text{III}}, \text{Te}^{\text{IV}}$); (e) $(\text{NH}_4)_{18}[(\text{NH}_4)_{12}(\text{UO}_2(\text{H}_2\text{O}))_6(\text{UO}_2(\mu_2\text{-H}_2\text{O}))_6(\alpha\text{-AsW}_9\text{O}_{34})_6] \cdot 74\text{H}_2\text{O}$; (f) $[\text{U}_4(\mu_3\text{-O})_2(\text{SiW}_9\text{O}_{34})_2(\text{CH}_3\text{COO})_2]^{10-}$; (g) $[(\text{U}^{\text{IV}})_{5.5}(\text{U}^{\text{VI}}\text{O})_{0.5}(\mu_3\text{-OH})_4(\mu_3\text{-O})_4(\text{OAc})_2(\text{AsW}_9\text{O}_{33})_3]^{19-}$; (h) $[(\text{U}^{\text{IV}})_3(\text{U}^{\text{VI}}\text{O})_3(\mu_3\text{-OH})_4(\mu_3\text{-O})_4(\text{AsW}_9\text{O}_{33})_3]^{15-}$; (i) $[(\text{U}^{\text{IV}})_6(\mu_3\text{-OH})_4(\mu_3\text{-O})_4(\text{AsW}_9\text{O}_{33})_4]^{24-}$; (j) $\{\text{Na}@\{(\text{SbW}_9\text{O}_{33})_2(\text{UO}_2)_6(\text{PO}_3\text{OH})_6\}\}^{17-}$; (k) $[(\text{K}(\text{OH}_2))_4(\text{UO}_2)_4(\text{OH})_2(\text{SiW}_{10}\text{O}_{36})_4]^{22-}$; (l) $[(\{\text{Na}(\text{OH}_2)\}_4(\text{UO}_2)_4(\text{OH})_2(\text{SiW}_{10}\text{O}_{36})_4]^{22-}$. Color codes: W, blue; U^{VI}, yellow; U^{IV}, light green; Na, dark grey; K, lavender; P, magenta; Si and Ge, orange; As, purple; Te^{IV}, pink; Sb^{III}, dark blue; O, red; C, light gray.

cent to each $\{\text{SiW}_{10}\}$ but K^+ ions are located at the positions in middle of two $\{\text{SiW}_{10}\}$.

Afterward, Pope reported two similar sandwich structures based on $\{\text{Sb}^{\text{III}}\text{W}_9\}$ and $\{\text{Te}^{\text{IV}}\text{W}_9\}$ (Fig. 1d).³⁵ In both structures of $[(\text{UO}_2)_2(\text{H}_2\text{O})_2(\text{SbW}_9\text{O}_{33})_2]^{14-}$ and $[(\text{UO}_2)_2(\text{H}_2\text{O})_2(\text{TeW}_9\text{O}_{33})_2]^{12-}$, the trivacant $\{\text{XW}_9\}$ only offered four of the six unsaturated terminal oxygen atoms to coordinate with two uranyl ions. Thus, the obtained sandwich structure showed a different “open” configuration (Fig. 1d). Besides, $[(\text{UO}_2)_2(\text{H}_2\text{O})_2(\text{TeW}_9\text{O}_{33})_2]^{12-}$ could also be *in situ* synthesized from simple raw materials including TeO_2 , $\text{UO}_2(\text{NO}_3)_2 \cdot 6\text{H}_2\text{O}$, $\text{Na}_2\text{WO}_4 \cdot 2\text{H}_2\text{O}$ and NH_4Cl . In 2005, David systematically studied and compared the spectra of several sandwich U-hetero-POWs with the general formulas of $[(\text{UO})_3(\text{H}_2\text{O})_6(\text{XW}_9\text{O}_{34})_2]^{12/14-}$ ($\text{X} = \text{P/Si/Ge}$) and $[\text{U}_3(\text{XW}_9\text{O}_{33})_2]^{6-}$ ($\text{X} = \text{As/Sb/Bi}$).⁷⁰ This work revealed the shifting law of bonds in these sandwich U-hetero-POWs and trivacant precursors $\{\text{XW}_9\}$.

Subsequently, Khoshnavazi also *in situ* synthesized three sandwich uranium-containing polytungstoarsenates using

HAc , $\text{Na}_2\text{WO}_4 \cdot 2\text{H}_2\text{O}$, $\text{Na}_2\text{HAsO}_4 \cdot 7\text{H}_2\text{O}$, and $\text{UO}_2(\text{OAc})_2 \cdot 2\text{H}_2\text{O}$.³⁶ The addition of NaCl , NH_4Cl , and KCl yielded $\text{Na}_{12}[\text{Na}_2\text{As}_2\text{W}_{18}\text{U}_2\text{O}_{72}] \cdot 35\text{H}_2\text{O}$, $(\text{NH}_4)_{13}[\text{NH}_4\text{As}_2\text{W}_{18}\text{U}_2\text{O}_{72}] \cdot 17\text{H}_2\text{O}$, and $\text{K}_{13}[\text{KAs}_2\text{W}_{18}\text{U}_2\text{O}_{72}] \cdot 10\text{H}_2\text{O}$, respectively. These U-hetero-POWs exhibited similar structures with the general formula $[\text{M}_2(\text{UO}_2)_2(\text{PW}_9\text{O}_{34})_2]^{12-}$ ($\text{M} = \text{Na, K, NH}_4$) reported by Pope as mentioned above (Fig. 1b and c). A Na salt based on $\{\text{BiW}_9\}$, which was similar to K^+ and NH_4^+ of $[\text{M}_2(\text{UO}_2)_2(\text{PW}_9\text{O}_{34})_2]^{12-}$, was also successfully obtained by Alizadeh and the formula was $[\text{Na}(\text{UO}_2)_2(\text{H}_2\text{O})_4(\text{BiW}_9\text{O}_{33})_2]^{13-}$.³⁸ In 2011, Mohadeszadeh synthesized a rare Keggin- $\{\text{As}^{\text{V}}\text{W}_9\}$ -based hexamer, $(\text{NH}_4)_{18}[(\text{NH}_4)_{12}(\text{UO}_2(\text{H}_2\text{O}))_6(\text{UO}_2(\mu_2\text{-H}_2\text{O}))_6(\alpha\text{-AsW}_9\text{O}_{34})_6] \cdot 74\text{H}_2\text{O}$, by the reaction of $(\text{NH}_4)_{13}[\text{NH}_4\text{As}_2\text{W}_{18}\text{U}_2\text{O}_{72}] \cdot 17\text{H}_2\text{O}$ and $(\text{NH}_4)_3\text{Ce}(\text{SO}_4)_4 \cdot 2\text{H}_2\text{O}$ in a $\text{pH} = 3.5$ solution (Fig. 1 and 2).³⁹ This hexameric polyanion is composed of six $\{\text{As}^{\text{V}}\text{W}_9\}$, six four-coordinated uranyl ions, and two trinuclear clusters $\{(\text{UO}_2)_3\}$. Each $\{\text{As}^{\text{V}}\text{W}_9\}$ is coordinated with three single uranyl ions and one $\{(\text{UO}_2)_3\}$ to form a cage configuration.

Four years later, Duval reported four $\{\text{SiW}_9\}$ -based POMs, among which a tetrานuclear $\{\text{U}^{\text{IV}}(\mu_3\text{-O})_2\}$ -based sandwich structure was constructed from two $\{\text{SiW}_9\}$ moieties (Fig. 1f).²⁸ It should be noted that $[\text{U}_4(\mu_3\text{-O})_2(\text{SiW}_9\text{O}_{34})_2(\text{CH}_3\text{COO})_2]^{10-}$ was synthesized using UCl_4 in a $\text{pH} = 4.7$ acetate buffer, instead of uranyl salts. However, one must admit that the combination of uranyl and acetate buffer is very difficult to control due to the fast formation and precipitation of $\text{Na}[\text{U}^{\text{VI}}\text{O}_2(\text{OAc})_3]$. The success of these U-hetero-POWs should be attributed to the usage of UCl_4 for assembly and quick separation before the formation of $\text{Na}[\text{U}^{\text{VI}}\text{O}_2(\text{OAc})_3]$. After this work, Duval also synthesized three multi-sandwich structures using a similar method (Fig. 1g-i).⁴⁰ Similar hexanuclear uranium clusters with different ratios of substitutional-disordered $\text{U}^{\text{IV}}/\text{U}^{\text{VI}}$ were stabilized by the coordination of three or four $\{\text{As}^{\text{III}}\text{W}_9\}$, *i.e.*, $[(\text{U}^{\text{IV}})_{5.5}(\text{U}^{\text{VI}}\text{O})_{0.5}(\mu_3\text{-OH})_4(\mu_3\text{-O})_4\text{O}(\text{OAc})_2(\text{AsW}_9\text{O}_{33})_3]^{19-}$, $[(\text{U}^{\text{IV}})_3(\text{U}^{\text{VI}}\text{O})_3(\mu_3\text{-OH})_4(\mu_3\text{-O})_4(\text{AsW}_9\text{O}_{33})_3]^{15-}$, and $[(\text{U}^{\text{IV}})_6(\mu_3\text{-OH})_4(\mu_3\text{-O})_4(\text{AsW}_9\text{O}_{33})_4]^{24-}$. The former two compounds were obtained from the same solution at different time. The degree of oxidation with time from U^{IV} to U^{VI} could be revealed from the formulas. By diluting the concentration of acetate buffer and raw materials, crystals of $\text{Na}_{24}[(\text{U}^{\text{IV}})_6(\mu_3\text{-OH})_4(\mu_3\text{-O})_4(\text{AsW}_9\text{O}_{33})_4] \cdot 42\text{H}_2\text{O}$ were obtained without $\text{Na}[\text{U}^{\text{VI}}\text{O}_2(\text{OAc})_3]$. In 2021, Kong and co-workers synthesized a novel sandwich structure $\text{Na}_{17}\{\text{Na}@\{[\text{SbW}_9\text{O}_{33}]_2(\text{UO}_2)_6(\text{PO}_3\text{OH})_6\}\} \cdot x\text{H}_2\text{O}$ ($x \approx 46$), which was built from Keggin- $\{\text{SbW}_9\}$ and the central $\{\text{Na}@\{(\text{UO}_2)_6(\text{PO}_3\text{OH})_6\}$ cluster (Fig. 1j).⁴¹ Two $\{\text{SbW}_9\}$ offered all six unsaturated terminal oxygen atoms for coordination with six uranyl ions. $\text{Na}_{17}\{\text{Na}@\{[\text{SbW}_9\text{O}_{33}]_2(\text{UO}_2)_6(\text{PO}_3\text{OH})_6\}\} \cdot x\text{H}_2\text{O}$ also has the biggest uranium clusters among those Keggin-type sandwich U-hetero-POWs. Besides, this compound is also synthesized by an *in situ* method from SbCl_3 , Na_2WO_4 , NaOAc , H_3PO_4 , and $\text{UO}_2(\text{NO}_3)_2 \cdot 6\text{H}_2\text{O}$.

2.1.2 Dawson-type structures. Dawson-type POMs are the second main category of POMs among thousands of derivative structures. However, the number of reported Dawson-type U-POMs to date is much lower than that of Keggin-type. Fewer Dawson-type precursors may be responsible for the lower number of Dawson-type U-hetero-POMs given the lacunary precursor synthesis strategy for the great majority of U-hetero-POMs. The first Dawson-type U-hetero-POWs were reported by Rusu and co-workers without crystal structures in 1999.⁷¹ But they provided the formulas, *i.e.*, $\text{Na}_{18}[(\text{UO})_3(\text{P}_2\text{W}_{15}\text{O}_{56})_2]$ and $\text{Na}_{18}[(\text{UO})_3(\text{H}_2\text{O})_6(\text{P}_2\text{W}_{15}\text{O}_{56})_2] \cdot 27\text{H}_2\text{O}$. The study of spectroscopy and isotope exchange experiments was carried out. The first Dawson-type U-hetero-POW with a definite structure was reported by Pope in 2003 (Fig. 3).⁴² The obtained $\text{Na}_{32}[(\text{UO}_2)_{12}(\mu_3\text{-O})_4(\mu_2\text{-H}_2\text{O})_{12}(\text{P}_2\text{W}_{15}\text{O}_{56})_4] \cdot 77\text{H}_2\text{O}$ product was synthesized using the vapor diffusion of CH_3CN into an aqueous solution of trivacant Dawson- $\{\text{P}_2\text{W}_{15}\}$ and $\text{UO}_2(\text{NO}_3)_2 \cdot 6\text{H}_2\text{O}$. In this polyanion, four groups of trinuclear uranyl clusters $\{(\text{UO}_2)_3(\mu_3\text{-O})(\mu_2\text{-H}_2\text{O})_3\}$ adopted a near-ideal centrosymmetric arrangement around the center of symmetry. Each trivacant Dawson- $\{\text{P}_2\text{W}_{15}\}$ offered six oxygen atoms to coordinate with three $\{(\text{UO}_2)_3(\mu_3\text{-O})(\mu_2\text{-H}_2\text{O})_3\}$. Thus, the tetrahedral structure was formed by the sandwiching of four

Dawson- $\{\text{P}_2\text{W}_{15}\}$ and four $\{(\text{UO}_2)_3(\mu_3\text{-O})(\mu_2\text{-H}_2\text{O})_3\}$. Solvent water molecules occupied the central hole in the polyanion.

In 2003, Antonio and Pope both reported a series of 1:2 sandwich structures based on U^{IV} and monovacant Dawson- $\{\text{P}_2\text{W}_{17}\}$ units with a similar formula of $[\text{U}(\text{P}_2\text{W}_{17}\text{O}_{61})_2]^{16-}$.^{43,44} Pope's work represented the case of diastereomers in U-POMs caused by the two isomers of $\{\text{P}_2\text{W}_{17}\}$, *i.e.*, $[\text{U}(\alpha_1\text{-P}_2\text{W}_{17}\text{O}_{61})_2]^{16-}$, $[\text{U}(\alpha_1\text{-P}_2\text{W}_{17}\text{O}_{61})(\alpha_2\text{-P}_2\text{W}_{17}\text{O}_{61})]^{16-}$, and $[\text{U}(\alpha_2\text{-P}_2\text{W}_{17}\text{O}_{61})_2]^{16-}$ (Fig. 4). P-NMR revealed the interconversion relationships of these compounds. Moisy also reported similar Dawson-type $\text{An}^{\text{IV}}(\alpha_2\text{-P}_2\text{W}_{17}\text{O}_{61})_2$ in 2009, including $[\text{U}(\alpha_2\text{-P}_2\text{W}_{17}\text{O}_{61})_2]^{16-}$ in the *syn*-conformation.⁴⁵

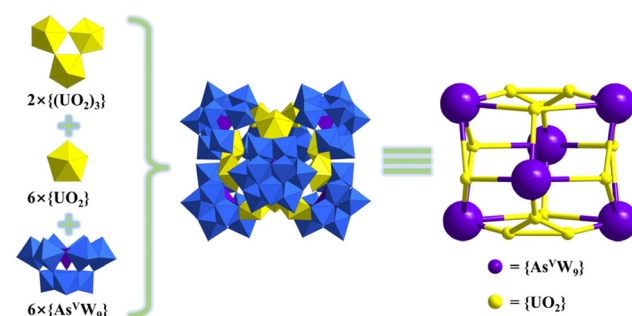


Fig. 2 Structural representation of $[(\text{NH}_4)_{12}(\text{UO}_2(\text{H}_2\text{O}))_6(\text{UO}_2(\mu_2\text{-H}_2\text{O}))_6(\alpha\text{-AsW}_9\text{O}_{34})]^{18-}$. Color codes are the same as in Fig. 1.

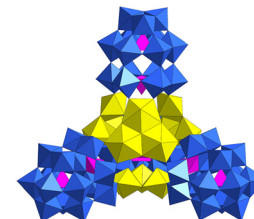


Fig. 3 View of $[(\text{UO}_2)_{12}(\mu_3\text{-O})_4(\mu_2\text{-H}_2\text{O})_{12}(\text{P}_2\text{W}_{15}\text{O}_{56})_4]^{32-}$. Color codes are the same as in Fig. 1.

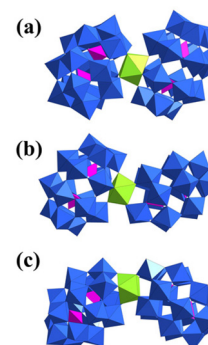


Fig. 4 Views of (a) $[\text{U}(\alpha_1\text{-P}_2\text{W}_{17}\text{O}_{61})_2]^{16-}$, (b) $[\text{U}(\alpha_1\text{-P}_2\text{W}_{17}\text{O}_{61})(\alpha_2\text{-P}_2\text{W}_{17}\text{O}_{61})]^{16-}$, and (c) $[\text{U}(\alpha_2\text{-P}_2\text{W}_{17}\text{O}_{61})_2]^{16-}$. Color codes are the same as in Fig. 1.

Chen and co-workers also reported a Dawson-like structure based on a half-open $\{\text{Si}_2\text{W}_{18}\}$ unit in 2007, *i.e.*, $\text{Na}_5[\text{K}[\text{UO}_2(\text{H}_2\text{O})_2(\text{A}-\alpha\text{-H}_3\text{SiW}_9\text{O}_{33})_2]]$.⁴⁶ A $\{\text{K}[\text{UO}_2(\text{H}_2\text{O})_2]\}$ cluster was captured by the open sites of half-open $\{\text{Si}_2\text{W}_{18}\}$, which was similar to Keggin-type dimeric structures. One year later, Kortz synthesized a novel horseshoe-shaped Dawson-type structure using $\text{K}_{16}\text{Li}_2[\text{H}_6\text{P}_4\text{W}_{24}\text{O}_{94}] \cdot 33\text{H}_2\text{O}$ ($\{\text{P}_4\text{W}_{24}\}$), $\text{UO}_2(\text{NO}_3)_2$, and $\text{pH} = 4$ LiOAc/HOAc buffer (Fig. 5a).⁴⁷ In the polyanion $[\text{Li}(\text{H}_2\text{O})\text{K}_4(\text{H}_2\text{O})_3\{(\text{UO}_2)_4(\text{O}_2)_4(\text{H}_2\text{O})_2\}_2(\text{PO}_3\text{OH})_2\text{P}_6\text{W}_{36}\text{O}_{136}]^{25-}$, two groups of tetranuclear uranyl peroxide clusters $\{(\text{UO}_2)_4(\text{O}_2)_4(\text{H}_2\text{O})_2\}$ were stabilized by the coordination of oxygen atoms offered by HPO_4^{2-} and “U”-shaped trimeric Dawson- $\{\text{P}_6\text{W}_{36}\}$, which was *in situ* assembled from the Dawson-type precursor $\{\text{P}_4\text{W}_{24}\}$. It is worth noting that the addition of 4–6 drops of H_2O_2 and low reaction temperature (50°C), which are usually used for the synthesis of uranyl peroxide clusters, may be the key factors for the synthesis of these POMs. However, it is a pity that there were no new Dawson-type U-POMs until ten years later. In 2019, Duval reported the first Dawson- $\{\text{P}_8\text{W}_{48}\}$ -based structure, $[(\text{UO}_2)_{7.2}(\text{HCOO})_{7.8}(\text{P}_8\text{W}_{48}\text{O}_{184})\text{Cl}_8]^{41.4-}$, among which chloride was assembled into the structures of U-hetero-POMs for the first time.⁴⁸ This compound is also the first U-POM synthesized using a hydrothermal method. The reaction of $\{\text{P}_8\text{W}_{48}\}$, LiCl , and $\text{UO}_2(\text{NO}_3)_2 \cdot 6\text{H}_2\text{O}$ in HCOONa buffer at 160°C gave a mixture of insoluble residue and a clear solution. Crystals of $(\text{K}_{11.3}\text{Li}_{8.1}\text{Na}_{22})[(\text{UO}_2)_{7.2}(\text{HCOO})_{7.8}(\text{P}_8\text{W}_{48}\text{O}_{184})\text{Cl}_8] \cdot 89\text{H}_2\text{O}$ could be obtained by the evaporation of this solution. It is known that there is a big typical central cavity within $\{\text{P}_8\text{W}_{48}\}$ and various relatively light metal ions or clusters can be captured in this cavity. But all the uranyl ions in $[(\text{UO}_2)_{7.2}(\text{HCOO})_{7.8}(\text{P}_8\text{W}_{48}\text{O}_{184})\text{Cl}_8]^{41.4-}$ are located on both sides of the $\{\text{P}_8\text{W}_{48}\}$ ring with disorder instead of in the central cavity. The occupancies of U1 and U2 are 0.25 and 0.65, respectively. Korenev and co-workers also reported two similar $\{\text{P}_8\text{W}_{48}\}$ -based structures in 2019, but the uranyl ions were even more disordered.⁴⁹ The formulas are $\text{K}_{24}[(\text{UO}_2)_8(\text{P}_8\text{W}_{48}\text{O}_{184})] \cdot 50\text{H}_2\text{O} \cdot 3\text{LiCl}$ and $(\text{NH}_4)_{16}\text{H}_8[(\text{UO}_2)_8(\text{P}_8\text{W}_{48}\text{O}_{184})] \cdot 50\text{H}_2\text{O}$. About one year later, Kortz synthesized a new $\{\text{P}_8\text{W}_{48}\}$ -based uranyl-peroxide-cluster-containing POW, $\text{K}_{18}\text{Li}_{22}[(\text{UO}_2)_4(\text{O}_2)_4\{(\text{P}_8\text{W}_{48}\text{O}_{184})\}] \cdot 133\text{H}_2\text{O}$, among which two groups of tetranuclear uranyl peroxide clusters $\{(\text{UO}_2)_4(\text{O}_2)_4\}$ were both

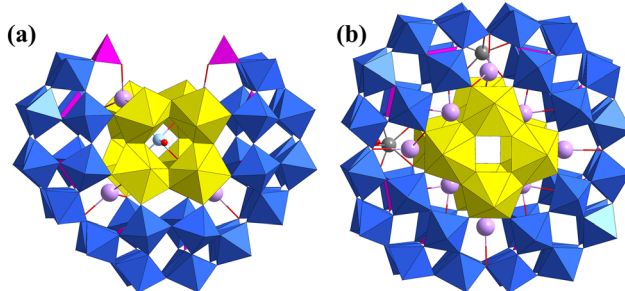


Fig. 5 Views of (a) $[\text{Li}(\text{H}_2\text{O})\text{K}_4(\text{H}_2\text{O})_3\{(\text{UO}_2)_4(\text{O}_2)_4(\text{H}_2\text{O})_2\}_2(\text{PO}_3\text{OH})_2\text{P}_6\text{W}_{36}\text{O}_{136}]^{25-}$ and (b) $\text{K}_{18}\text{Li}_{22}[(\text{UO}_2)_4(\text{O}_2)_4\{(\text{P}_8\text{W}_{48}\text{O}_{184})\}] \cdot 133\text{H}_2\text{O}$. Color codes are the same as in Fig. 1; Li, pale blue.

located in the central cavity of $\{\text{P}_8\text{W}_{48}\}$ (Fig. 5b).⁵⁰ This is also the first case in which such heavy atom clusters were assembled in the central cavity of $\{\text{P}_8\text{W}_{48}\}$. Several potassium ions were also captured in the central cavity.

Recently, our group and Zhang's group reported the first two uranium-containing selenotungstates based on tetravacant Dawson- $\{\text{Se}_2\text{W}_{14}\}$ (Fig. 6).⁵¹ The reaction of $\text{Na}_2\text{WO}_4 \cdot 2\text{H}_2\text{O}$, Na_2SeO_3 , and $\text{UO}_2(\text{NO}_3)_2 \cdot 6\text{H}_2\text{O}$ in an aqueous solution yielded two sandwich-type Dawson POWs, *i.e.*, $\text{Na}_3[\text{H}_{19}(\text{UO}_2)_2(\mu_2\text{-O})(\text{Se}_2\text{W}_{14}\text{O}_{52})_2] \cdot 41\text{H}_2\text{O}$ and $(\text{NH}_4)_{10}[\text{H}_4(\text{SeO})_2(\text{UO}_2)_2(\text{H}_2\text{O})_2(\text{H}_2\text{Se}_2\text{W}_{14}\text{O}_{52})(\text{Se}_2\text{W}_{14}\text{O}_{52})] \cdot 66\text{H}_2\text{O}$. In the former one, two $\{\alpha\text{-Se}_2\text{W}_{14}\}$ sandwiched four halves of positionally disordered uranyl. In the latter polyanion, two $\{\gamma\text{-Se}_2\text{W}_{14}\}$ sandwiched two uranyl and two $\{\text{Se}^{IV}\text{O}\}$. It is also worth noting that this work represents two rare *in situ* synthesis cases among U-hetero-POMs. Different pH and counter cations ($(\text{CH}_3)_2\text{NH}\cdot\text{HCl}$ and NH_4Cl) were the significant factors of the one-pot synthesis procedures.

2.1.3 Silverton-type structures. The Silverton-type structures are one of the earliest U-hetero-POMs to be studied.⁹ All these Silverton-type U-hetero-POMs are based on the typical Silverton-type $(\text{UMo}_{12}\text{O}_{42})^{8-}$ anion. To the best of our knowledge, these Silverton-type $\{\text{UMo}_{12}\}$ -based POMs were all reported by Torchenkova and co-workers from the former Soviet Union during 1981–1990 (Fig. 7).^{15,52–59} Different metal ions, including Sc^{3+} , VO^{2+} , Fe^{3+} , Ni^{2+} , Cu^{2+} , Nd^{3+} , Er^{3+} , Th^{4+} , and UO_2^{2+} ,

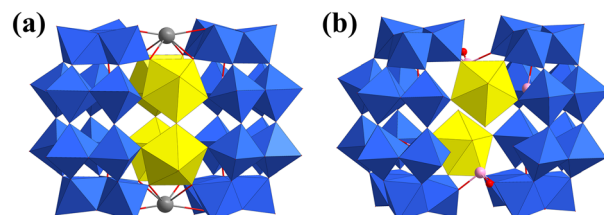


Fig. 6 Views of (a) $[(\text{UO}_2)_2(\mu_2\text{-O})(\text{Se}_2\text{W}_{14}\text{O}_{52})_2]^{22-}$ and (b) $[(\text{SeO})_2(\text{UO}_2)_2(\text{H}_2\text{O})_2(\text{H}_2\text{Se}_2\text{W}_{14}\text{O}_{52})(\text{Se}_2\text{W}_{14}\text{O}_{52})]^{14-}$. Se^{IV} , pink; other color codes are the same as in Fig. 1.

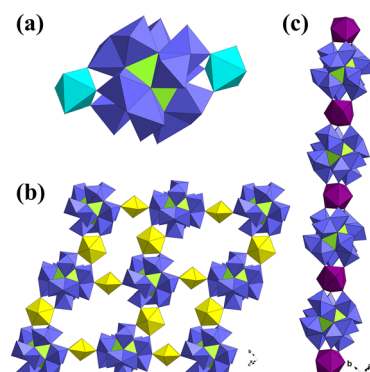


Fig. 7 Views of the Silverton-type $\{\text{UMo}_{12}\}$ -based structures. (a) $[(\text{VO})_2(\text{H}_2\text{O})_4(\text{UMo}_{12}\text{O}_{42})]^{4-}$; (b) $[(\text{UO}_2)_2(\text{H}_2\text{O})_3(\text{UMo}_{12}\text{O}_{42})]^{4-}$; (c) $[\text{Th}(\text{H}_2\text{O})_3(\text{UMo}_{12}\text{O}_{42})]^{4-}$. Color codes: Mo, blue; U^{IV} , light green; U^{VI} , yellow; Th^{IV} , violet; V, turquoise.

were incorporated into the structure by the coordination of three terminal oxygen atoms of $\{\text{UMo}_{12}\}$ with a similar formula of $\{\text{M}_a(\text{H}_2\text{O})_b(\text{UMo}_{12}\text{O}_{42})\}^{c-}$ ($a = 1$ or 2 ; $b = 0, 3, 4, 6, 12$; $c = 2$ or 4). However, most of them are 0D structures, only Th^{4+} and UO_2^{2+} incorporated compounds showed extended structures. $[\text{Th}(\text{H}_2\text{O})_3(\text{UMo}_{12}\text{O}_{42})]^{4-}$ is a 1D chain built from Th^{4+} and $\{\text{UMo}_{12}\text{O}_{42}\}^{8-}$, alternately. $[(\text{UO}_2)_2(\text{H}_2\text{O})_3(\text{UMo}_{12}\text{O}_{42})]^{4-}$ represented a rare inorganic (4,4)-connected 2D network if $\{\text{UMo}_{12}\}$ clusters were regarded as nodes.

2.1.4 Hybrid structures. Loosely, there are only four cases that are constructed from more than one basic building block to date. The first was one of the three similar triangular sandwich structures reported by Pope in 2001, *i.e.*, $[(\text{UO}_2)_3(\text{H}_2\text{O})_5\text{As}_3\text{W}_{29}\text{O}_{104}]^{19-}$, $[(\text{UO}_2)_3(\text{H}_2\text{O})_6\text{As}_3\text{W}_{30}\text{O}_{105}]^{15-}$, and $[(\text{UO}_2)_3(\text{H}_2\text{O})_6\text{As}_3\text{W}_{29}\text{V}^{\text{IV}}\text{O}_{105}]^{17-}$ (Fig. 8a–c).⁶⁰ The first one $[(\text{UO}_2)_3(\text{H}_2\text{O})_5\text{As}_3\text{W}_{29}\text{O}_{104}]^{19-}$ could be viewed as a hybrid structure based on a Keggin- $\{\text{AsW}_9\}$ and a Dawson-like $\{\{\text{AsW}_9\}_2(\text{W}_2)\}$ unit, which was *in situ* transformed from $\text{Na}_{27}[\text{NaAs}_4\text{W}_{40}\text{O}_{140}] \cdot 60\text{H}_2\text{O}$ (Fig. 8a). The other two compounds were classified as cryptand structures. The second case of a hybrid structure was reported by Pope in 2002.³⁴ The reaction of $\text{Na}_9[\text{AsW}_9\text{O}_{33}] \cdot 27\text{H}_2\text{O}$ and $\text{UO}_2(\text{NO}_3)_2 \cdot 6\text{H}_2\text{O}$ in an aqueous solution resulted in the formation of $(\text{NH}_4)_{17}[(\text{UO}_2)_3(\text{H}_2\text{O})_4\text{As}_3\text{W}_{26}\text{O}_{94}] \cdot 16\text{H}_2\text{O}$ and part of Keggin- $\{\text{AsW}_9\}$ *in situ* transformed into Dawson-like $\{\text{As}_2\text{W}_{17}\}$ (Fig. 8d). This $\{\text{As}_2\text{W}_{17}\}$ unit is not the classical monovacant Dawson- $\{\text{As}_2\text{W}_{17}\}$ and is built from two rare Keggin- $\{\text{AsW}_8\}$ units and one bridging $\{\text{WO}_6\}$. As a result, one $\{\text{AsW}_8\}$ and one $\{\text{As}_2\text{W}_{17}\}$ sandwiched three uranyl to form a triangle configuration. The third one is an iso-heteropolytungstate, $[(\text{H}_3\text{SbW}_{17}\text{O}_{59})\text{U}^{\text{IV}}(\text{HW}_5\text{O}_{18})]^{11-}$, which was constructed from a monovacant Lindqvist- $\{\text{W}_5\}$ and a monovacant Dawson- $\{\text{Sb}^{\text{III}}\text{W}_{17}\}$.⁶¹ Significantly, this compound was synthesized from simple materials and is the first case of an *in situ* synthesized U-POM as far as we know.

Recently, our group and Zhang's group reported a new uranium-containing selenotungstate that consisted of one Anderson- $\{\text{SeW}_6\}$ unit and three Keggin- $\{\text{SeW}_9\}$ units (Fig. 9).⁶²

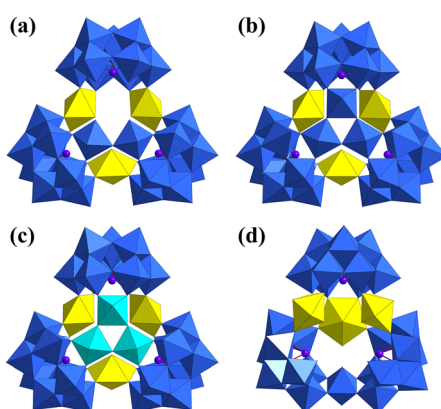


Fig. 8 Views of (a) $[(\text{UO}_2)_3(\text{H}_2\text{O})_5\text{As}_3\text{W}_{29}\text{O}_{104}]^{19-}$, (b) $[(\text{UO}_2)_3(\text{H}_2\text{O})_6\text{As}_3\text{W}_{30}\text{O}_{105}]^{15-}$, (c) $[(\text{UO}_2)_3(\text{H}_2\text{O})_6\text{As}_3\text{W}_{29}\text{V}^{\text{IV}}\text{O}_{105}]^{17-}$, and (d) $[(\text{UO}_2)_3(\text{H}_2\text{O})_4\text{As}_3\text{W}_{26}\text{O}_{94}]^{17-}$. Color codes are the same as in Fig. 1.

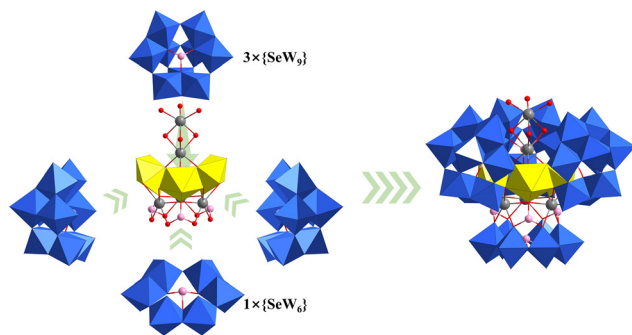


Fig. 9 View of $[(\text{UO}_2)_3(\text{SeO}_3)_3\text{Na}_5(\text{H}_2\text{O})_6(\text{SeW}_6\text{O}_{21})(\text{SeW}_9\text{O}_{33})_3]^{21-}$. Color codes are the same as in Fig. 6.

In this hybrid polyanion, $[(\text{UO}_2)_3(\text{SeO}_3)_3\text{Na}_5(\text{H}_2\text{O})_6(\text{SeW}_6\text{O}_{21})(\text{SeW}_9\text{O}_{33})_3]^{21-}$, a rare $\{\text{Se}_3\text{U}_3\text{Na}_5\}$ cluster was surrounded by one Anderson- $\{\text{SeW}_6\}$ and three Keggin- $\{\text{SeW}_9\}$ units from four directions to form a bouquet-like structure. This Anderson- $\{\text{SeW}_6\}$ is different from traditional Anderson units and can be viewed as a derivative of Keggin- $\{\text{SeW}_{12}\}$ removing the top and the bottom $\{\text{W}_3\}$ units. This compound was also a rare case of an *in situ* synthesized U-POM.

2.1.5 Cryptand structures. Compared with lacunary POMs, cryptand POMs show more rigid coordination sites. Meanwhile, the assembly ability of cryptand POMs is also limited by their stability and the sizes of open sites. The Preyssler-type $[\text{P}_5\text{W}_{30}\text{O}_{110}]^{15-}$ ($\{\text{P}_5\text{W}_{30}\}$) is a typical cryptand POM and is also one of the earliest models used to study the reactions between POMs and actinides. In 1993, Pope used $\{\text{P}_5\text{W}_{30}\}$ to capture various transition metal ions.⁷² The U^{4+} ion was successfully assembled in the central cavity of $\{\text{P}_5\text{W}_{30}\}$ by ion exchange under high-temperature reflux conditions (140–180 °C). Three years later, Pope reported a similar ammonium salt with a formula of $(\text{NH}_4)_{11}[\text{U}(\text{H}_2\text{O})\text{P}_5\text{W}_{30}\text{O}_{110}] \cdot 12\text{H}_2\text{O}$ (Fig. 10).⁶³ Single-crystal data revealed the positional disorder of U^{4+} within the cavity. The U^{4+} ion and an additional H_2O are located on the C_5 axis of $\{\text{P}_5\text{W}_{30}\}$. Compared with the U^{4+} ion, the central H_2O was closer to the central position.

Another typical cryptand POM is $[\text{As}_4\text{W}_{40}\text{O}_{140}]^{28-}$ ($\{\text{As}_4\text{W}_{40}\}$).⁷³ $\{\text{As}_4\text{W}_{40}\}$ exhibits two kinds and five in total coordination sites, theoretically. These two kinds of coordination sites are called S1 (the only one positioned at the center

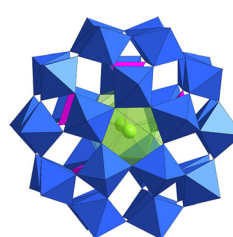


Fig. 10 View of $[\text{U}(\text{H}_2\text{O})\text{P}_5\text{W}_{30}\text{O}_{110}]^{11-}$. Color codes are the same as in Fig. 1.

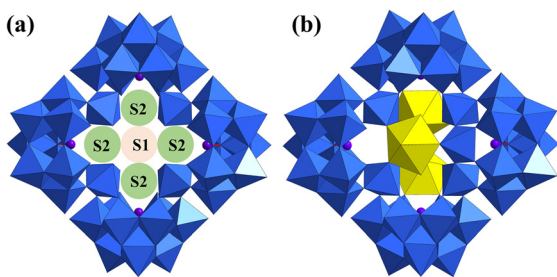


Fig. 11 Views of (a) two kinds of coordination sites S1 and S2 in $\{\text{As}_4\text{W}_{40}\}$ and (b) $[\text{Na}(\text{UO}_2)_3(\text{OH})(\text{H}_2\text{O})_6\text{As}_4\text{W}_{40}\text{O}_{140}(\text{WO})]^{18-}$. Color codes are the same as in Fig. 1.

of $\{\text{As}_4\text{W}_{40}\}$) and S2 (doubled at two positions between two opposite $\{\text{AsW}_9\}$ sub-units) (Fig. 11a). The first $\{\text{As}_4\text{W}_{40}\}$ -based structure was one of the five cases of U-hetero-POMs reported by Pope in 2002 (Fig. 11b).³⁴ The tetramer $[\text{Na}(\text{UO}_2)_3(\text{OH})(\text{H}_2\text{O})_6\text{As}_4\text{W}_{40}\text{O}_{140}(\text{WO})]^{18-}$ was synthesized from UCl_4 and $\text{Na}_{27}[\text{NaAs}_4\text{W}_{40}\text{O}_{140}] \cdot 60\text{H}_2\text{O}$ and crystallized from solution at room temperature. However, only three uranyl were assembled in the open sites of $\{\text{As}_4\text{W}_{40}\}$. U1 and U2 at S2 in this structure were both coordinated by two unsaturated oxygen sites from the $\{\text{AsW}_9\}$ part of $\{\text{As}_4\text{W}_{40}\}$, two single H_2O , and a $\mu_2\text{-OH}$. But U3 exhibited positional disorder with a 5-coordinated W atom at another two S2 sites.

It is interesting to note that the three $\{\text{As}_4\text{W}_{40}\}$ -based U-hetero-POMs were also synthesized using UCl_4 and $\text{Na}_{27}[\text{NaAs}_4\text{W}_{40}\text{O}_{140}] \cdot 60\text{H}_2\text{O}$ by Duval in 2018 (Fig. 12).⁶⁴ By changing the amounts of UCl_4 or $\{\text{As}_4\text{W}_{40}\}$, three similar tetramers were obtained from a similar $\text{HCOONa}/\text{HCOOH}$ buffer at room temperature, namely $[\{\text{U}_2(\mu_2\text{-OH})_3(\mu_2\text{-O})\}\text{As}_4\text{W}_{40}\text{O}_{140}]^{25-}$, $[\{\text{U}_2(\mu_2\text{-O})(\text{HCOO})_3\}\text{As}_4\text{W}_{40}\text{O}_{140}]^{25-}$, and $[\{\text{U}_4(\mu_2\text{-O})_2(\text{HCOO})_4\}\text{As}_4\text{W}_{40}\text{O}_{140}]^{20-}$. But the U^{4+} ions in $[\{\text{U}_2(\mu_2\text{-OH})_3(\mu_2\text{-O})\}\text{As}_4\text{W}_{40}\text{O}_{140}]^{25-}$ were all positionally disordered with 0.5 occupancy for each S2 position. In $[\{\text{U}_2(\mu_2\text{-O})(\text{HCOO})_3\}\text{As}_4\text{W}_{40}\text{O}_{140}]^{25-}$, two U^{4+} ions were connected by three $\mu_2\text{-formate}$ and a $\mu_2\text{-O}$ at two S2 positions. One of the $\{\text{AsW}_9\}$ sub-units was also transformed into a different configuration. The four U^{4+} ions in $[\{\text{U}_4(\mu_2\text{-O})_2(\text{HCOO})_4\}\text{As}_4\text{W}_{40}\text{O}_{140}]^{20-}$ were all located at S2 sites and an additional Na^+ was also assembled at the S1 site.

Besides, the above-mentioned $[(\text{UO}_2)_3(\text{H}_2\text{O})_6\text{As}_3\text{W}_{30}\text{O}_{105}]^{15-}$ and $[(\text{UO}_2)_3(\text{H}_2\text{O})_6\text{As}_3\text{W}_{29}\text{V}^{\text{IV}}\text{O}_{105}]^{17-}$ could also be viewed as

cryptand-based structures (Fig. 8b and c).⁶⁰ Three $\{\text{AsW}_9\}$ were linked by $\{\text{W}_3\}$ and $\{\text{VW}_2\}$ to form new $\{\text{As}_3\text{W}_{30}\}$ and $\{\text{As}_3\text{W}_{29}\text{V}\}$ building units with a triangular configuration. Three uranyl ions were coordinated by the oxygen atoms of the open sites. It was notable that the three atoms in $\{\text{VW}_2\}$ exhibited positional disorder and the occupancies of V and W were 1/3 and 2/3 in total, respectively. The other cryptand-based structures were the four $\{\text{P}_8\text{W}_{48}\}$ -based structures as mentioned in section 2.1.2.

2.2 U-oxo-clusters

U-oxo-clusters discussed in this review are those structures that could be defined as POMs and uranium and oxygen atoms are the main building units of the structures. Uranium shows unique self-assembly modes in aqueous solution, which are distinctly different from traditional POMs built from early TM (W, Mo, etc.). Uranyl ions are always assembled into capsule-like uranyl peroxide clusters or other similar uranyl-oxo-clusters in the presence of H_2O_2 or other organic or inorganic ligands, while tetravalent uranium is easy to hydrolyze into U^{IV} -oxo-clusters with various structures. It is worth noting that there are no known U^{IV} -containing peroxide clusters due to rapid oxidation caused by H_2O_2 . Burns is the pioneer in the field of actinide oxo-clusters, especially uranyl peroxide clusters, and Nyman also made outstanding contributions in this field.^{10,74-76} One finds that the chemistry of uranyl peroxide clusters has already developed into a significant field from structure-driven to deeper research of chemical behaviors and has broadened the scope of POMs.⁷⁷⁻⁸⁰ The U-oxo-clusters discussed in this section were mainly reported in recent years.

2.2.1 Uranyl peroxide clusters and POM-related uranyl peroxide phosphate clusters. Most of the uranyl peroxide clusters can also be called uranyl peroxide capsules due to their hollow-shell structures and uranyl peroxide rings or crowns. Various organic and inorganic ligands have been used as linkers of the clusters among those uranyl peroxide clusters. The organic ligands are mainly various organic phosphoric acids as well as oxalic acid (ox). Sun summarized the structural chemistry of uranium phosphonates based on the structures of organic phosphonate ligands and the hetero-metals.⁸¹ Inorganic ligands include PO_4^{3-} , HPO_3^{2-} , $\text{P}_2\text{O}_7^{4-}$ (Pp), NO_3^- , WO_4^{2-} , MoO_4^{2-} , and other anions in addition to O_2^{2-} . Those previously reported uranyl peroxide clusters from $\{\text{U}_{16}\}$ to $\{\text{U}_{124}\}$ showed abundant topologies but could also be divided into two categories.⁷⁶ The first kind of uranyl peroxide clusters built only from uranyl ions, O_2^{2-} , and OH^- are the most typical representatives of uranyl peroxide capsules. The biggest case is the highly symmetrical $\{\text{U}_{60}\}$ cluster $[(\text{UO}_2(\text{O}_2)(\text{OH}))_{60}]^{60-}$. These kinds of uranyl peroxide capsules could be viewed as the combination of 4/5/6-membered uranyl polygons or bigger secondary building units (SBUs) of $\{(\text{UO}_2)_x(\text{O}_2)_x\}$ by sharing edges. The other kinds of uranyl peroxide clusters are those clusters in which different $\{(\text{UO}_2)_x(\text{O}_2)_x\}$ SBUs are linked by various organic and inorganic ligands as mentioned above. In consideration of the concept of polyoxometalates, only those structures with typical clusters are discussed here. These

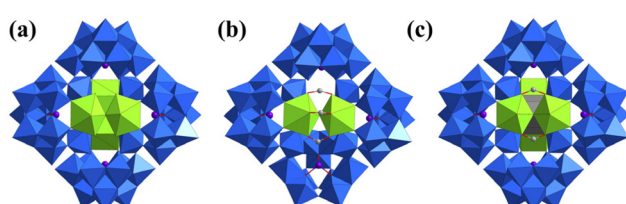


Fig. 12 Views of (a) $[(\text{U}_2(\mu_2\text{-OH})_3(\mu_2\text{-O}))\text{As}_4\text{W}_{40}\text{O}_{140}]^{25-}$, (b) $[(\text{U}_2(\mu_2\text{-O})(\text{HCOO})_3)\text{As}_4\text{W}_{40}\text{O}_{140}]^{25-}$, and (c) $[(\text{U}_4(\mu_2\text{-O})_2(\text{HCOO})_4)\text{As}_4\text{W}_{40}\text{O}_{140}]^{20-}$. Color codes are the same as in Fig. 1.

Table 2 Summary of typical uranyl peroxide clusters

Codes	Formula	Shape	SBUs of clusters	Ref.
$\{U_{16}\}$	$[(UO_2)_{16}(O_2)_{24}(OH)_8]^{24-}$	Bowl-like	$\{U_4\}$ quadrangle, $\{U_6\}$ hexagon	82
$\{U_{16}(hedp)_8\}$	$[(UO_2)_{16}(O_2)_{16}(hedp)_8]^{32-}$	Cage	$\{U_4\}$ ring, $\{U_8\}$ double ring	83
$\{U_{16}(hedp)_8P_4\}$	$[(UO_2)_{16}(O_2)_8(OH)_8[(hedp)_8(PO_4)_4]^{28-}$	Cage	$\{U_4\}$ ring, $\{(UO_2)_2(OH)_2\}$	83
$\{U_{18}Pp_2Pcp_6\}$	$[(UO_2)_{18}(O_2)_{18}(OH)_2(Pcp)_6(Pp)_2]^{34-}$	Cage	$\{U_8\}$ double ring, $\{U_{10}\}$ ring	84
$\{U_{18}Pp_6\}$	$[(UO_2)_{18}(O_2)_{18}(OH)_4(Pp)_6(H_2O)_4]^{28-}$	Cage	$\{U_8\}$ double ring, $\{U_{10}\}$ triple ring	85
$\{U_{19}(Ppb)_4\}$	$[(UO_2)_{19}(O_2)_{26}(OH)_2(Ppb)_4]^{32-}$	Cage	$\{U_8\}$ double ring, $\{U_{11}\}$ triple ring	86
$\{U_{20}\}$	$[(UO_2)_{20}(O_2)_{30}]^{20-}$	Cage	$\{U_5\}$ pentagon	87
$\{U_{20R}\}$	$[(UO_2)_{20}(OH)_{16}(O_2)_{28}]^{32-}$	Crown-like	$\{U_5\}$ pentagon	82
$\{U_{20}P_6\}$	$[(UO_2)_{20}(O_2)_{27}(HPO_4)_6]^{26-}$	Cage	$\{U_5\}$, $\{U_8\}$ ring	88
$\{U_{20}P_{12}\}$	$[(UO_2)_{20}(O_2)_{24}(HPO_4)_6(H_2PO_4)_6]^{26-}$	Cage	$\{U_8\}$ ring	88
$\{U_{20}Pp_6a\}$	$[(UO_2)_{20}(O_2)_{24}(Pp)_6]^{32-}$	Cage	$\{U_{10}\}$ triple ring	84
$\{U_{20}Pp_6b\}$	$[(UO_2)_{20}(O_2)_{24}(Pp)_6]^{32-}$	Cage	$\{U_5\}$, $\{U_{10}\}$ ring	84
$\{U_{20}Pp_{10}\}$	$[(UO_2)_{20}(O_2)_{20}(Pp)_{10}]^{40-}$	Cage	$\{U_8\}$ double ring, $\{U_{12}\}$ quadruple ring	84
$\{U_{20}Pp_{10a}\}$	$[(UO_2)_{20}(O_2)_{20}(Pp)_{10}]^{40-}$	Cage	$\{U_5\}$, $\{U_{10}\}$ ring	85
$\{U_{20}(hedp)_{10}\}$	$[(UO_2)_{20}(O_2)_{20}[(hedp)_10]^{40-}$	Cage	$\{U_5\}$, $\{(UO_2)_{10}(O_2)_{10}\}$ rings	83
$\{U_{20}(Ppb)_{10}\}$	$[(UO_2)_{20}(O_2)_{20}(Ppb)_{10}]^{40-}$	Cage	$\{U_5\}$, $\{U_{10}\}$ ring	89
$\{U_{20}(Ppb)_6\}$	$[(UO_2)_{20}(O_2)_{24}(Ppb)_6]^{32-}$	Cage	$\{U_{10}\}$ triple ring	89
$\{U_{21}Pp_9\}$	$[(UO_2)_{21}(O_2)_{21}(Pp)_9(OH)_3]^{39-}$	Cage	$\{U_4\}$ ring, $\{U_9\}$ triple ring	85
$\{U_{22p}\}$	$[(UO_2)_{22}(O_2)_{15}(HPO_3)_{20}(H_2O)_{10}]^{26-}$	Cage	$\{U_4\}$ ring, $\{U_2\}$	90
$\{U_{24}\}$	$[(UO_2)_{24}(OH)_{24}(O_2)_{24}]^{24-}$	Cage	$\{U_4\}$ quadrangle, $\{U_6\}$ hexagon	91
$\{U_{24R}\}$	$[(UO_2)_{24}(OH)_{36}(O_2)_{12}]^{24-}$	Crown-like	$\{U_6\}$ hexagon	82
$\{U_{24}Pp_9\}$	$[(UO_2)_{24}(O_2)_{25}(Pp)_9(OH)_4]^{42-}$	Cage	$\{U_4\}$ ring, $\{U_8\}$ double ring, $\{U_{12}\}$ triple ring	85
$\{U_{24}Pcp_{10}\}$	$[(UO_2)_{24}(O_2)_{24}(Pcp)_{10}(H_2O)_4]^{40-}$	Cage	$\{U_4\}$, $\{U_8\}$ rings	85
$\{U_{24}Pp_{12}\}$	$[(UO_2)_{24}(O_2)_{24}(Pp)_{12}]^{48-}$	Cage	$\{U_4\}$ ring	84
$\{U_{24}Pcp_{12}\}$	$[(UO_2)_{24}(O_2)_{24}(Pcp)_{12}]^{48-}$	Cage	$\{U_4\}$ ring	84
$\{U_{24}(hedp)_{12}\}$	$[(UO_2)_{24}(O_2)_{24}[(hedp)_{12}]^{48-}$	Cage	$\{U_4\}$ ring	83
$\{U_{26}Pp_6\}$	$[(UO_2)_{26}(O_2)_{33}(Pp)_6]^{38-}$	Cage	$\{U_5\}$ pentagon	84
$\{U_{26}Pp_{11}\}$	$[(UO_2)_{26}(O_2)_{28}(Pp)_{11}]^{48-}$	Cage	$\{U_5\}$ ring, $\{(UO_2)_{16}\}$ triple ring	84
$\{U_{26}(Ppb)_6\}$	$[(UO_2)_{26}(O_2)_{33}(Ppb)_6]^{38-}$	Cage	$\{U_5\}$ pentagon, $\{U_6\}$ hexagon	89
$\{U_{28}\}$	$[(UO_2)_{28}(O_2)_{42}]^{28-}$	Cage	$\{U_5\}$ pentagon, $\{U_6\}$ hexagon	91
$\{U_{28a}\}$	$[(UO_2)_{28}(O_2)_{28}(OH)_{28}]^{28-}$	Cage	$\{U_4\}$ quadrangle, $\{U_5\}$ pentagon, $\{U_6\}$ hexagon	92
$\{U_{28p}\}$	$[(UO_2)_{28}(O_2)_{20}(HPO_3)_{24}(H_2O)_{12}]^{32-}$	Cage	$\{(UO_2)_4(O_2)_4\}$, $\{(UO_2)_2(O_2)\}$	90
$\{U_{30}\}$	$[(UO_2)_{30}(O_2)_{36}(OH)_{22}]^{34-}$	Cage	$\{U_4\}$ quadrangle, $\{U_5\}$ pentagon, $\{U_6\}$ hexagon	92
$\{U_{30a}\}$	$[(UO_2)_{30}(O_2)_{30}(OH)_{30}]^{30-}$	Cage	$\{U_4\}$ quadrangle, $\{U_5\}$ pentagon, $\{U_6\}$ hexagon	93
$\{U_{30}Pp_6\}$	$[(UO_2)_{30}(O_2)_{39}(Pp)_6]^{42-}$	Cage	$\{U_6\}$ ring, Bowl-like $\{U_{24}\}$: $\{U_5\}$ pentagon, $\{U_6\}$ hexagon	93
$\{U_{30}Pp_{10}Ox_5\}$	$[(UO_2)_{30}(O_2)_{30}(Pp)_{10}(Ox)_5]^{50-}$	Cage	$\{U_5\}$, $\{U_{10}\}$ rings	94
$\{U_{30}Pp_{12}P\}$	$[(UO_2)_{30}(O_2)_{30}(Pp)_{12}(PO_4)(H_2O)_5]^{51-}$	Double cage	$\{U_5\}$, $\{U_{10}\}$ rings	93
$\{U_{32}\}$	$[(UO_2)_{32}(OH)_{32}(O_2)_{32}]^{32-}$	Cage	$\{U_4\}$ quadrangle, $\{U_5\}$ pentagon, $\{U_6\}$ hexagon	91
$\{U_{32R}\}$	$[(UO_2)_{32}(O_2)_{40}(OH)_{24}]^{40-}$	Crown-like	$\{U_5\}$ pentagon, $\{U_6\}$ hexagon	95
$\{U_{32}Pp_{16}\}$	$[(UO_2)_{32}(O_2)_{32}(Pp)_{16}]^{64-}$	Cage	$\{U_4\}$ ring	84
$\{U_{36}\}$	$[(UO_2)_{36}(O_2)_{41}(OH)_{26}]^{36-}$	Cage	$\{U_5\}$ pentagon, $\{U_6\}$ hexagon	96
$\{U_{36a}\}$	$[(UO_2)_{36}(O_2)_{36}(OH)_{36}]^{36-}$	Cage	$\{U_4\}$ quadrangle, $\{U_5\}$ pentagon, $\{U_6\}$ hexagon	92
$\{U_{36}Ox_6\}$	$[(UO_2)_{36}(O_2)_{48}(Ox)_6]^{36-}$	Cage	Bowl-like $\{U_{18}\}$ septuple ring	97
$\{U_{38}Pp_{10}Nt_4\}$	$[(UO_2)_{38}(O_2)_{40}(Pp)_{10}(NO_3)_4]^{56-}$	Cage	$\{U_8\}$ double ring, $\{U_{11}\}$ triple ring	94
$\{U_{40}\}$	$[(UO_2)_{40}(OH)_{40}(O_2)_{40}]^{40-}$	Cage	$\{U_4\}$ quadrangle, $\{U_5\}$ pentagon, $\{U_6\}$ hexagon	98
$\{U_{40}(hedp)_{20}\}$	$[(UO_2)_{40}(O_2)_{40}[(hedp)_20]^{80-}$	Cage	$\{U_4\}$ ring	83
$\{U_{42}\}$	$[(UO_2)_{42}(O_2)_{42}(OH)_{42}]^{42-}$	Cage	$\{U_4\}$ quadrangle, $\{U_5\}$ pentagon, $\{U_6\}$ hexagon	93
$\{U_{42}Pp_3\}$	$[(UO_2)_{42}(O_2)_{42}(OH)_{36}(Pp)_3]^{48-}$	Cage	$\{U_4\}$ quadrangle, $\{U_5\}$ pentagon, $\{U_6\}$ hexagon, $\{U_{10}\}$ decagon	93
$\{U_{44}\}$	$[(UO_2)_{44}(O_2)_{66}]^{44-}$	Ellipsoid cage	$\{U_5\}$ pentagon, $\{U_6\}$ hexagon	96
$\{U_{44a}\}$	$[(UO_2)_{44}(O_2)_{44}(OH)_{44}]^{44-}$	Dumbbell-like	$\{U_4\}$ quadrangle, $\{U_6\}$ hexagon, $\{U_8\}$ octagon	92
$\{U_{45}Pp_{23}\}$	$[(UO_2)_{45}(O_2)_{44}(Pp)_{23}]^{90-}$	Cage	$\{U_4\}$, $\{U_5\}$ rings, $\{(UO_2)_3(O_2)_2\}$	83
$\{U_{50}\}$	$[(UO_2)_{50}(OH)_{50}(O_2)_{50}]^{50-}$	Cage	$\{U_5\}$ pentagon, $\{U_6\}$ hexagon	98
$\{U_{50}Ox_{20}\}$	$[(UO_2)_{50}(O_2)_{43}(OH)_4(Ox)_{20}]^{30-}$	Cage	$\{U_5\}$ ring, $\{U_8\}$ double ring	99
$\{U_{54}Pp_{27}\}$	$[(UO_2)_{54}(O_2)_{54}(Pp)_{27}]^{108-}$	Cage	$\{U_4\}$, $\{U_5\}$ rings	85
$\{U_{60}\}$	$[(UO_2)_{60}(O_2)_{60}(OH)]^{60-}$	Cage	$\{U_5\}$ pentagon, $\{U_6\}$ hexagon	96
$\{U_{60}Ox_{30}\}$	$[(UO_2)_{60}(O_2)_{60}(Ox)_{30}]^{60-}$	Cage	$\{U_5\}$ ring	97
$\{U_{64}(hedp)_{32}\}$	$[(UO_2)_{64}(O_2)_{64}(hedp)_{32}]^{128-}$	Cage	$\{U_4\}$ ring	83

Table 2 (Contd.)

Codes	Formula	Shape	SBUs of clusters	Ref.
{U ₂₈ U _{40R} } or {U ₆₈ }	[(UO ₂) ₆₈ (O ₂) ₇₄ (OH) ₁₆ (NO ₃) ₁₆ (H ₂ O) ₁₆] ⁴⁴⁻	{U ₂₈ } cage {U _{40R} } saddle-like ring	{U ₂₈ }:{U ₅ } pentagon, {U ₆ } hexagon; {U _{40R} }:{U ₄ } quadrangle, {U ₅ } pentagon	100
{U ₁₂₀ O ₉₀ } {U ₁₂₄ P ₃₂ }	[(UO ₂) ₁₂₀ (O ₂) ₁₂₀ (Ox) ₉₀] ¹⁸⁰⁻ [(UO ₂) ₁₂₄ (O ₂) ₁₅₂ (PO ₄) ₁₆ (HPO ₄) ₈ (H ₂ PO ₄) ₈ (OH) ₂ (H ₂ O) ₂₄] ¹³²⁻	Double-layer cage Five cages combined structure	{U ₅ } rings Bowl-like {U ₁₈ } septuple ring, {U ₁₆ } triple ring, {U ₅ } ring	99 101

Abbreviation: hedp = (1-hydroxyethane-1,1-diyl)bis(phosphonic acid), Pcp = methylenebis(phosphonic acid), Ppb = benzene-1,2-diphosphonic acid.

uranyl peroxide clusters could be classified according to the numbers of uranyl moieties in the cluster and then their topologies. The typically reported uranyl peroxide clusters are summarized in Table 2.⁷⁶ Those uranyl peroxide clusters containing other TM ions are classified in section 2.2.2. Being different from traditional POMs, the counter cations are found to be one of the most important factors influencing the assembly progress, structures, states of aggregation, and solubilities of uranyl peroxide clusters, sometimes even more important than pH.^{6,76,102} The attractiveness of uranyl peroxide clusters is not only their varied topology but also the interesting space chemistry within the inner cavities of the cages.^{103,104}

In 2017, Burns synthesized the only two uranyl peroxide phosphate clusters with $\mu\eta^1\cdot\eta^2$ peroxide bridges, $\text{Li}_4\text{Na}_{12}\{(\text{SO}_4)\text{CNa}_{12}\text{C}[(\text{UO}_2)_{20}(\text{O}_2)_{27}(\text{HPO}_4)_6]\}$ and $\text{Li}_x\text{Na}_{16-x}\{(\text{SO}_4)\text{CNa}_{12}\text{C}[(\text{UO}_2)_{20}(\text{O}_2)_{24}(\text{HPO}_4)_6(\text{H}_2\text{PO}_4)_6]\}$ (Fig. 13). Different amounts of Na_2SO_3 and H_3PO_4 and different basic pH values resulted in the two similar but different uranyl peroxide phosphate clusters. The inner cores were both $\{\text{Na}_{12}(\text{SO}_4)\}$ clusters, which were further surrounded by different fullerene-like $\{\text{U}_{20}\}$ phosphate shells.⁸⁸ At the end of 2018, Burns reported six new uranyl peroxide phosphate clusters, and $\text{P}_2\text{O}_7^{4-}$ and methylenebis(phosphonic acid) $[(\text{CH}_2)(\text{PO}_3\text{H}_2)_2]$, Pcp were used as bridging ligands (Fig. 14).⁸⁵ The obtained $\{\text{U}_{18}\text{Pp}_6\}$, $\{\text{U}_{20}\text{Pp}_{10a}\}$, $\{\text{U}_{21}\text{Pp}_9\}$, $\{\text{U}_{24}\text{Pp}_9\}$, $\{\text{U}_{24}\text{Pcp}_{10}\}$, and $\{\text{U}_{54}\text{Pp}_{27}\}$ show different topologies of uranyl peroxide clusters, which were constructed from different SBUs of clusters linked by $\text{P}_2\text{O}_7^{4-}$ or Pcp ligands. The compositions of these uranyl peroxide phosphate clusters are summarized in Table 3.

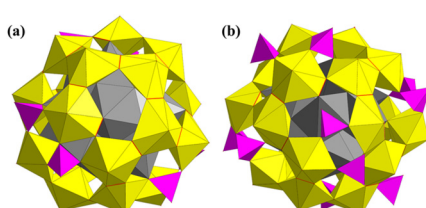


Fig. 13 Views of (a) $\text{Li}_4\text{Na}_{12}\{(\text{SO}_4)\text{CNa}_{12}\text{C}[(\text{UO}_2)_{20}(\text{O}_2)_{27}(\text{HPO}_4)_6]\}$ and (b) $\text{Li}_x\text{Na}_{16-x}\{(\text{SO}_4)\text{CNa}_{12}\text{C}[(\text{UO}_2)_{20}(\text{O}_2)_{24}(\text{HPO}_4)_6(\text{H}_2\text{PO}_4)_6]\}$. Color codes are the same as in Fig. 1.

Burns also used high-temperature drop solution calorimetry to study the enthalpies of formation of several uranyl peroxide clusters and the disassembly and assembly process from $\text{Li}_{24}\text{Na}_{24}\{[(\text{UO}_2)(\text{O}_2)]_{24}(\text{P}_2\text{O}_7)_{12}\}$ to $\text{Li}_{24}\{(\text{UO}_2)(\text{O}_2)(\text{OH})\}_{24}$ and a series of uranyl peroxide clusters containing $\{\text{U}_{24}\text{Pp}_{12}\}$, $\{\text{U}_{26}\text{Pp}_6\}$, $\{\text{U}_{28}\}$, $\{\text{U}_{22}(\text{PO}_3)_{20}\}$, and $\{\text{U}_{28}(\text{PO}_3)_{24}\}$ with different counter cations.^{105,106} Then, the transformation from stadtite to different uranyl peroxide clusters was also investigated. The chains of uranyl peroxide polyhedra in stadtite, $[(\text{UO}_2)(\text{O}_2)(\text{H}_2\text{O})_2](\text{H}_2\text{O})_2$, were converted into two kinds of uranyl peroxide clusters under different conditions, *i.e.*, $\{\text{U}_{28}\}$ and $\{\text{U}_{20}\}$, which was revealed by Raman spectra and electrospray ionization mass spectrometry (ESI-MS).¹⁰⁷ Whereafter, a novel uranyl peroxide cluster, $\text{K}_{32}(\text{UO}_2)_{19}(\text{O}_2)_{26}(\text{OH})_2(\text{Ppb})_4\cdot65\text{H}_2\text{O}$ (Ppb = benzene-1,2-diphosphonic acid), was synthesized with a new “open oyster” structure. Abundant hydrogen bonds, $\pi\cdots\pi$, and K···π interactions, and K–O bonds supported the formation of the supramolecular structures. This $\{\text{U}_{19}\}$ cluster could also transform into a typical $\{\text{U}_{24}\}$ cage, $\text{K}_{24}(\text{UO}_2)_{24}(\text{O}_2)_{24}(\text{OH})_{24}\cdot n\text{H}_2\text{O}$, with an octanuclear K-cluster within the central cavity.⁸⁶ The reaction of Ppb and $\text{UO}_2(\text{NO}_3)_2$ in a basic solution could also result in three new organic–inorganic hybrid uranyl peroxide clusters $[(\text{UO}_2)_{20}(\text{O}_2)_{20}(\text{Ppb})_{10}]^{40-}$, $[(\text{UO}_2)_{26}(\text{O}_2)_{33}(\text{Ppb})_6]^{38-}$, and $[(\text{UO}_2)_{20}(\text{O}_2)_{24}(\text{Ppb})_6]^{32-}$.⁸⁹ The two $\{\text{U}_{20}\}$ clusters both showed similar fullerene topology, while the $\{\text{U}_{26}\}$ cluster exhibited a distorted polyhedron with more than 15 faces. Nyman investigated the influence of three organic solvents (acetone, CH_3CN , and EtOH) in the synthesis of different fragments of uranyl peroxide clusters.⁷⁹ A new Anderson-like hexameric cluster, $\{\text{K}@\{(\text{UO}_2)_6(\text{O}_2)_9(\text{OH})_6\}\}$, was successfully isolated, which was the second stable ligand-free SBU of normal uranyl peroxide clusters (Fig. 15a). The first one, pentameric $\{\text{K}@\{(\text{UO}_2)_5(\text{O}_2)_5\}\}$, was also reported by Nyman in 2019 (Fig. 15b).¹⁰⁸ Besides, Forbes also synthesized a hexameric $\{(\text{UO}_2)_6(\text{O}_2)_6(\text{HPO}_4)_6\}$ in the absence of H_2O_2 (Fig. 15c).¹⁰⁹ An interesting peroxide process occurred with the help of trace levels of benzaldehyde and air. The raw material (aminomethyl)phosphonic acid *in situ* transformed into HPO_4^{2-} in the solution of methanol and benzyl alcohol with NaOH.

At the end of 2021, LaVerne and co-workers investigated the solid-state transformations of $\text{Ca}_{22}[\text{UO}_2(\text{O}_2)_3]\cdot 9\text{H}_2\text{O}$ and $\text{Li}_4[\{(\text{UO}_2)(\text{O}_2)_3\}\cdot 10\text{H}_2\text{O}$ under γ -irradiation.¹¹⁰ Single-crystal and

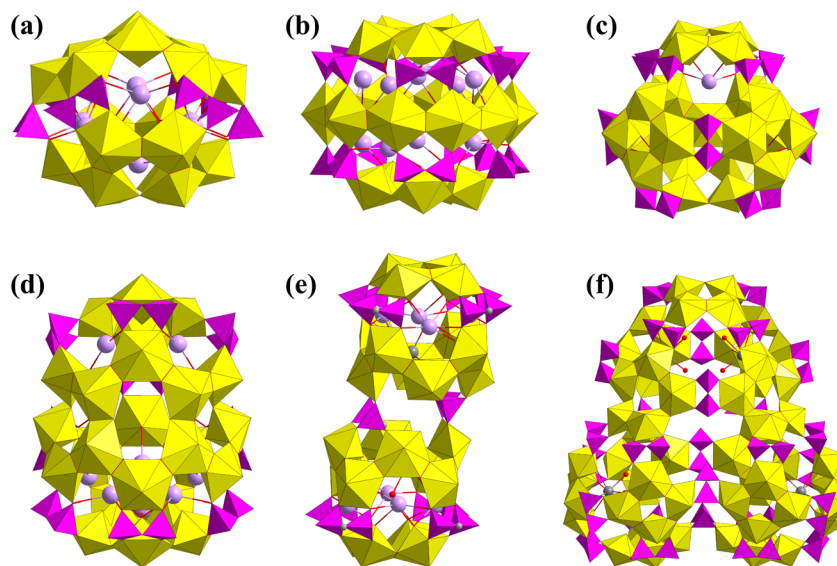


Fig. 14 Views of (a) $\{U_{18}Pp_6\}$, (b) $\{U_{20}Pp_{10a}\}$, (c) $\{U_{21}Pp_9\}$, (d) $\{U_{24}Pp_9\}$, (e) $\{U_{24}Pcp_{10}\}$, and (f) $\{U_{54}Pp_{27}\}$. Color codes are the same as in Fig. 1.

Table 3 Summary of the structures of $\{U_{18}Pp_6\}$, $\{U_{20}Pp_{10a}\}$, $\{U_{21}Pp_9\}$, $\{U_{24}Pp_9\}$, $\{U_{24}Pcp_{10}\}$, and $\{U_{54}Pp_{27}\}$

Codes	Formula	SBUs of clusters	Linkers
$\{U_{18}Pp_6\}$	$[(UO_2)_{18}(O_2)_{18}(OH)_4(P_2O_7)_6(H_2O)_4]^{28-}$	$\{(UO_2)_8(O_2)_8\}$, $\{(UO_2)_{10}(O_2)_{10}\}$	$6 P_2O_7^{4-}$
$\{U_{20}Pp_{10a}\}$	$[(UO_2)_{20}(O_2)_{20}(P_2O_7)_{10}]^{40-}$	$2 \times \{(UO_2)_5(O_2)_5\}$, $\{(UO_2)_{10}(O_2)_{10}\}$ ring	$2 \times 5 P_2O_7^{4-}$
$\{U_{21}Pp_9\}$	$[(UO_2)_{21}(O_2)_{21}(P_2O_7)_9(OH)_3]^{39-}$	$3 \times \{(UO_2)_4(O_2)_4\}$, $\{(UO_2)_9(O_2)_9\}$	3 and $6 P_2O_7^{4-}$
$\{U_{24}Pp_9\}$	$[(UO_2)_{24}(O_2)_{25}(P_2O_7)_9(OH)_4]^{42-}$	$\{(UO_2)_4(O_2)_4\}$, $\{(UO_2)_8(O_2)_8\}$, $\{(UO_2)_{12}(O_2)_{12}\}$	$9 P_2O_7^{4-}$
$\{U_{24}Pcp_{10}\}$	$[(UO_2)_{24}(O_2)_{24}(O_3PCH_2PO_3)_10(H_2O)_4]^{40-}$	$2 \times \{(UO_2)_4(O_2)_4\}$, $2 \times \{(UO_2)_8(O_2)_8\}$ ring	2×4 and $2 Pcp^{4-}$
$\{U_{54}Pp_{27}\}$	$[(UO_2)_{54}(O_2)_{54}(P_2O_7)_{27}]^{108-}$	$11 \times \{(UO_2)_4(O_2)_4\}$, $2 \times \{(UO_2)_5(O_2)_5\}$	$27 P_2O_7^{4-}$

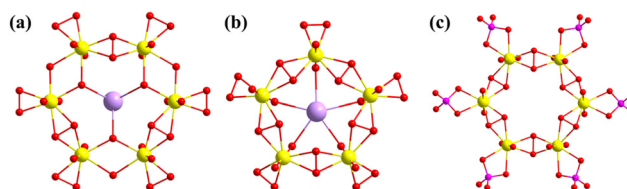


Fig. 15 Views of (a) $\{K@[(UO_2)_6(O_2)_9(OH)_6]\}$, (b) $\{K@[(UO_2)_5(O_2)_5]\}$, and (c) $\{[(UO_2)_6(O_2)_6(HPO_4)_6]\}$. Color codes are the same as in Fig. 1.

powder X-ray diffraction and Raman spectra revealed the different decomposition of peroxide groups into hydroxyl groups, which was influenced by Ca^{2+} and Li^+ . For $Ca_2[(UO_2)(O_2)_3] \cdot 9H_2O$, the products were a mixture of amorphous uranium phase and $Ca(OH)_2$. The product of $Li_4[(UO_2)(O_2)_3] \cdot 10H_2O$ was uranyl oxyhydrate. Very recently, Burns also used γ -ray radiation to promote the conversion of $Li_4[(UO_2)(O_2)_3]$ into $Li_{24}[(UO_2)(O_2)(OH)]_{24}$ in aqueous solutions.¹¹¹ They used *ex situ* Raman spectroscopy and ^{18}O labeling to track this transformation and found the dependence relationship between $Li_4[(UO_2)(O_2)_3]$, intermediates of uranyl peroxide clusters, and the radiation dose. These two works show us direct cases to understand the formation mechanism of POMs from monomer to derived species.

2.2.2 U-oxo-clusters containing other transition metals. This kind of U-oxo-cluster is mainly structures incorporating other TM ions. The introduction of a TM into U-oxo-clusters could result in more abundant coordination and connection modes. Burns synthesized a series of U-oxo-cluster phosphates incorporating Mo or W in 2014.¹¹² In these U-oxo-clusters, different uranyl peroxide clusters were connected by phosphate tetrahedra and Mo- or W-polyhedra to form different cage structures that showed similar corresponding uranyl peroxide clusters topologies, which were named $\{U_{18}W_2P_{12}\}$, $\{U_{28}W_4P_{12}\}$, $\{U_{28}Mo_4P_{12}\}$, $\{U_{44}Mo_2P_{16}\}$, $\{U_{48}W_6P_{48}\}$, and $\{U_{50}W_6P_{20}\}$. The number of UO_2^{2+} increased from 18 to 50. Mo- or W-polyhedra all served as linkers at the peaks in place of uranyl. Besides, all these compounds were synthesized in typical acidulous or circumneutral aqueous solutions containing H_3PO_4 , H_2O_2 , and $LiOH$. The dissociation of $H_3PMo_{12}O_{40}$ or $H_3PW_{12}O_{40}$ provided the corresponding MoO_4^{2-} or WO_4^{2-} ions.

In 2015, Burns reported two uranyl-vanadium oxide clusters, $[(UO_2)_2(V_{16}O_{46})]^{8-}$ and $[(UO_2)_{20}(V_2O_7)_{10}(SO_4)_{10}]^{20-}$ (Fig. 16).¹¹³ The $\{U_2V_{16}\}$ cluster could be viewed as a substitution product of the $\{V_{18}\}$ cluster with two uranyl ions. The $\{U_{20}V_{20}\}$ cluster represents a unique nano uranyl-vanadium wheel. Ten uranyl pentagonal bipyramids are connected by

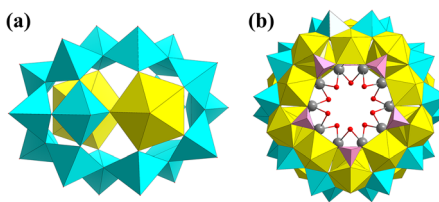


Fig. 16 Views of (a) $[(\text{UO}_2)_2(\text{V}_{16}\text{O}_{46})]^{8-}$ and (b) $[(\text{UO}_2)_{20}(\text{V}_2\text{O}_7)_{10}(\text{SO}_4)_{10}]^{20-}$. Color codes: U, yellow; V, turquoise; Na, dark grey; S, pink; O, red.

sharing vertices to form two pentagon-like $\{\text{U}_{10}\}$ rings. The two $\{\text{U}_{10}\}$ rings are further stabilized by the zigzag $\{\text{V}_{20}\}$ ring and SO_4^{2-} to build the unique wheel. Additional symmetric ten halves of Na ions are captured by the cavity of the wheel. One year later, Burns reported the first uranium–vanadium–phosphorus peroxide cage cluster with a formula of $[(\text{UO}_2)_{48}(\text{O}_2)_{12}(\text{VO}_5)_6(\text{PO}_4)_{48}]^{x-}$ ($x \approx 102$), which showed an iso-structure to $\{\text{U}_{48}\text{W}_6\text{P}_{48}\}$ reported in 2014.¹¹⁴ Subsequently, Burns synthesized an organic–inorganic hybrid uranium–iron cage cluster from a solution containing $\text{UO}_2(\text{NO}_3)_2$, H_2O_2 , LiOH , 3,3-diphosphono-propanoic acid (C_3P_2), and FeCl_3 (Fig. 17).¹¹⁵ One C_3P_2 was oxidized to the ligand 2,2-bis(phosphonato)acetate (C_2P_2) to combine with one Fe^{3+} . Three Fe^{3+} were connected by PO_4^{3-} and three $\mu_2\text{-OH}$ to form a trinuclear cluster $\{\text{Fe}_3(\text{OH})_3(\text{PO}_4)(\text{C}_2\text{P}_2)\}$. Four uranyl were connected by four $\mu_2\text{-O}_2^{2-}$ to form a $\{(\text{UO}_2)_4(\text{O}_2)_4\}$ cluster. Thus, eight $\{\text{Fe}_3(\text{OH})_3(\text{PO}_4)(\text{C}_2\text{P}_2)\}$ clusters and six $\{(\text{UO}_2)_4(\text{O}_2)_4\}$ clusters were connected by the phosphate groups of C_2P_2 to form the cage cluster $[\text{Li}_8(\text{UO}_2)_{24}(\text{FeOH})_{24}(\text{O}_2)_{24}(\text{PO}_4)_8(\text{C}_2\text{P}_2)_{24}]^{88-}$. This cage could be simplified as a nonstandard quadrangular dodecahedron if Fe trimers and U tetramers were considered as 3- and 4-connected nodes, respectively.

In 2019, Nyman investigated the influence of different counter cations on the hydrolysis of $\text{U}(\text{SO}_4)_2$ and a series of U^{IV} -oxo-sulfate clusters were obtained based on 6-, 70-, or 84-nuclear U^{IV} -oxo-clusters (Fig. 18).^{116,117} Lanthanides from La to Ho (except Pm) resulted in the formation of ten similar clusters of $[\text{U}_6(\text{OH})_4(\text{O})_4(\text{SO}_4)_{12}]^{12-}$ ($\{\text{U}_6\}$). While heavy lanthanides and Y^{3+} with smaller ionic radii resulted in a kind of hollow supercluster with more than 84 uranium atoms based on a body-centered-like cubic cluster, $\{[\text{U}_6(\text{OH})_4(\text{O})]_{14}(\text{SO}_4)_x\}$

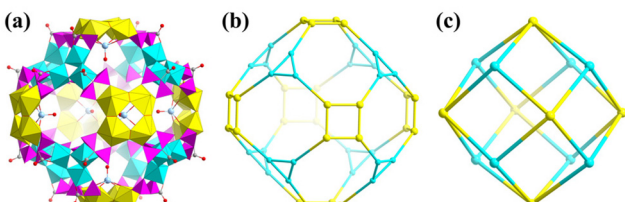


Fig. 17 Views of (a) $[\text{Li}_8(\text{UO}_2)_{24}(\text{FeOH})_{24}(\text{O}_2)_{24}(\text{PO}_4)_8(\text{C}_2\text{P}_2)_{24}]^{88-}$, (b) the simplified diagram, and (c) the simplified quadrangular dodecahedron. Color codes: U, yellow; Fe, turquoise; O, red; P, pink; C, gray; Li, pale blue.

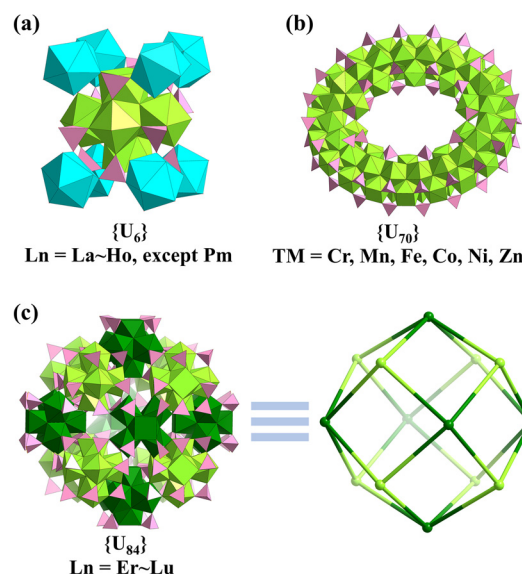


Fig. 18 Views of the (a) $\{\text{U}_6\}$, (b) $\{\text{U}_{70}\}$, and (c) $\{\text{U}_{84}\}$ clusters. Color codes: U^{IV} and $\{\text{U}_6\}$ units, light green and dark green; lanthanides and TM ions, turquoise; S, pink; O, red.

($\{\text{U}_{84}\}$, $x = 108$ for Y, 111 for Er, and 110 for Lu). The introduction of TM ions (Cr, Mn, Fe, Co, Ni, Zn) could yield wheel-shaped clusters of $[\text{U}_{70}(\text{OH})_{36}(\text{O})_{64}(\text{SO}_4)_{64}]^{12-}$ ($\{\text{U}_{70}\}$). Different counter cations and amounts of raw materials also led to different connection modes of these clusters. This series of U-oxo-clusters could also be classified as U-oxo-clusters due to the +4 valence of all the uranium atoms.

In 2021, Burns developed two kinds of uranyl vanadates with core–shell structures, which could be classified as U-oxo-clusters containing other transition metals (Fig. 19).¹¹⁸ $\{\text{U}_8\text{V}_6\}$

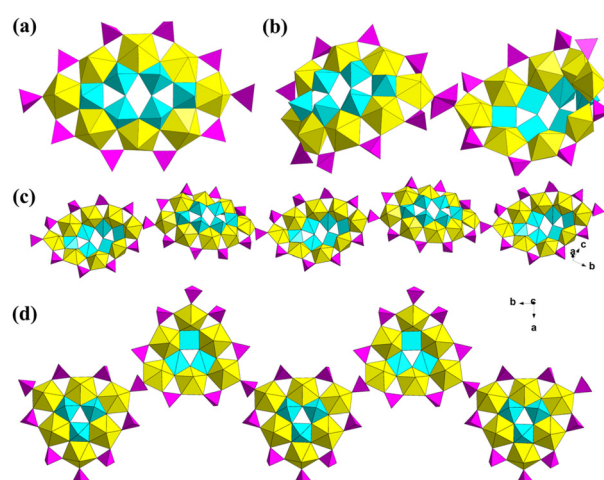


Fig. 19 Views of the (a) monomer, (b) dimer, and (c) 1D chain of $\{\text{U}_8\text{V}_6\}$ and (d) 1D chain of $\{\text{U}_6\text{V}_3\}$. In the $\{\text{U}_8\text{V}_6\}$ dimer, the $\{\text{PO}_4\}$ linker is represented with positional disorder. Carbon atoms for diethyl phosphate are omitted for simplicity. Color codes: U, yellow; V, turquoise; P, magenta; O, red.

and $\{U_6V_3\}$ could be obtained with different extended structures from an ionic liquid solution containing 1-ethyl-3-methylimidazolium diethyl phosphate (EMIm-Et₂PO₄), UO₂(NO₃)₂, NaVO₃, and/or VOSO₄, and Na₂WO₄. The monomer, dimer, and 1D chain of $\{U_8V_6\}$ and 1D chain of $\{U_6V_3\}$ represent a new series of U-oxo-clusters incorporating vanadium atoms.

2.2.3 U^{IV}-oxo-clusters and mixed-valence U-oxo-clusters. U-oxo-clusters built from low valence U^{IV} are usually obtained from the hydrolyzation of U^{IV} salts or the reduction of uranyl under specific conditions. Due to the similarity of some +4 metal ions, U^{IV} could assemble into a hexanuclear U^{IV}-cluster $\{U_6O_4(OH)_4\}$ or $\{U_6O_8\}$,^{119,120} which was similar to the $\{Zr_6O_4(OH)_4\}$ cluster in the famous metal-organic framework UiO-66. Various ligands were used to stabilize these U-oxo-clusters, such as carboxylic and N-heterocyclic ligands. Considering the correlation to the theme of this review, those metal-organic compounds with U-oxo-clusters that could be viewed as coordination polymers or metal-organic frameworks are not discussed here and other metal-organic U-oxo-clusters are selectively discussed.^{27,121-126}

Salmon and co-workers solvothermally synthesized a novel octanuclear U^{IV}-oxo-cluster, $(Hpy)_2[U_8L_4Cl_{10}O_4] \cdot 10py$ ($H_4L = N,N'$ -bis(3-hydroxysalicylidene)-1,2-phenylenediamine) as early as 2004 (Fig. 20).¹²⁷ This octanuclear cluster could be viewed as a combination of two parallelogram-like tetranuclear clusters linked by four μ_3 -O atoms and further stabilized by four Schiff base ligands, two μ_2 -Cl, and eight terminal Cl ions. In 2016, Mazzanti and co-workers isolated a star-shaped U-oxo-cluster, among which five uranyl ions and a pentavalent uranium atom were linked by bridging μ_3 -O linkers to form a pentagram configuration (Fig. 21a and b).¹²⁸ The photolytic reduction of uranyl resulted in these mixed-valence U-oxo-clusters. Two similar mixed-valence U-oxo-clusters, $[U(UO_2)_5(\mu_3-O)_5(PhCOO)_5(Py)_7]$ and $[U(UO_2)_5(\mu_3-O)_5(PhCOO)_5(Py)_7][UO_2(PhCOO)_2(Py)_2] \cdot 2Py$, were synthesized using a photolysis procedure with UO₂(NO₃)₂ in pyridine and the vapor diffusion of hexane into the pyridine reaction mixture. Besides, they also obtained a $\{U_{12}^{IV}U_4^V\}$ cluster, $\{[K(Py)_2]_2[K(Py)]_2[U_{16}O_{24}(PhCOO)_{24}(Py)_2]\}$, using a similar method (Fig. 21c and d). A similar $\{U_{12}^{IV}U_4^V\}$ cluster, $\{[K(MeCN)]_2[U_{16}O_{22}(OH)_2(PhCOO)_{24}]\} \cdot 4MeCN$, was also reported by Mazzanti in 2011 (Fig. 21e and f).¹²⁹ In this work, they also synthesized two similar $\{U_{10}\}$ clusters

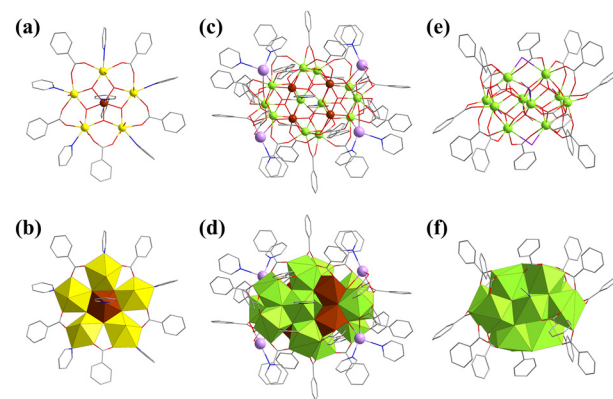


Fig. 21 Views of (a and b) $[U(UO_2)_5(\mu_3-O)_5(PhCOO)_5(Py)_7]$, (c and d) $\{[K(Py)_2]_2[K(Py)]_2[U_{16}O_{24}(PhCOO)_{24}(Py)_2]\}$, (e and f) $[U_{10}O_8(OH)_6(PhCO_2)_{14}I_4(H_2O)_2(MeCN)_2]$. Color codes: U^{IV}, green; U^V, brown; U^{VI}, yellow; I, violet. Other color codes are the same as in Fig. 1.

using $[U^{III}I_3(THF)_4]$ as the uranium source, *i.e.*, $[U_{10}O_8(OH)_6(PhCO_2)_{14}I_4(H_2O)_2(MeCN)_2]$ and $[U_{10}O_8(OH)_6(PhCO_2)_{12.79}I_{3.2}(H_2O)_4(MeCN)_4]_2I \cdot 4MeCN$. The average valence of uranium atoms should be +4 according to the bond valence sum (BVS) results and charge balance.

In 2018, Knope and co-workers synthesized a $\{U_6O_4(OH)_4\}$ -based 4-hydroxybenzoate, $U_6O_4(OH)_4(4\text{-HB})_{12}(H_2O)_6 \cdot 12H_2O$ (4-HB = 4-hydroxybenzoate), and another similar Th-cluster under a nitrogen atmosphere.¹³⁰ $U_6O_4(OH)_4(4\text{-HB})_{12}(H_2O)_6 \cdot 12H_2O$ is a typical 0D U^{IV}-oxo-cluster stabilized by ligands. They comprehensively investigated the structural chemistry of these two clusters *via* various means. Lin and co-workers investigated the influence of counter ions (Na^+ to Cs^+) in the assembly of U^{IV}-oxo-sulfate clusters.¹³¹ Na^+ and Rb^+ induced the formation of 0D $\{U_6O_4(OH)_4\}$ clusters with different packing structures, but Cs^+ resulted in a different trinuclear $\{U_3(\mu_3-O)\}$ -based 2D lamellar structure. These U^{IV}-oxo-sulfates were synthesized by the reduction of uranyl in an aqueous solution with Zn amalgam. Nyman also synthesized a $\{U_6\}$ -based cluster ($U(H_2O)_{4.5}U_6(OH)_4(O_4SO_4)_{10}(H_2O)_9$ using $U(SO_4)_2$ (Fig. 22).¹³² Each $\{U_6O_4(OH)_4\}$ cluster was coordinated with 12 SO_4^{2-} and connected with four single U^{IV}. Thus, a 4-connected *dia*-like 3D structure was constructed through the symmetrical extension of $\{U_6O_4(OH)_4\}$ clusters and single U^{IV} atoms.

In addition to the above $\{U_6O_4(OH)_4\}$ cluster, the hydrolyzation of UCl_4 could also yield U^{IV}-oxo-clusters with bridging Cl

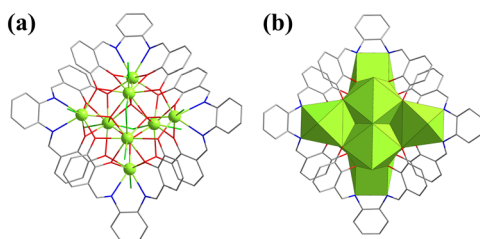


Fig. 20 (a) Ball-and-stick and (b) polyhedral views of $[U_8L_4Cl_{10}O_4]^{2-}$. Color codes: U^{IV}, light green; Cl, bright green; C, gray; O, red; N, dark blue.

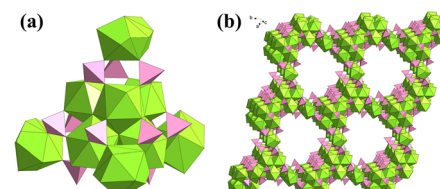


Fig. 22 Views of the (a) monomer and (b) three-dimensional structure of $(U(H_2O)_{4.5})_2U_6(OH)_4(O_4SO_4)_{10}(H_2O)_9$. Color codes: U^{IV}, green; S, pink; O, red.

ions. Knope synthesized a series of multinuclear uranium clusters under solvothermal conditions.¹³³ UCl_4 hydrolyzed into four U-oxo-clusters in a solution of THF with a little water, *i.e.*, $[\text{U}_4\text{Cl}_{10}\text{O}_2(\text{THF})_6(2\text{-FA})_2]\cdot 2(\text{THF})$, $[\text{U}_6\text{O}_4(\text{OH})_4(\text{H}_2\text{O})_3(2\text{-FA})_{12}]\cdot 7(\text{THF})\cdot(\text{H}_2\text{O})$, $[\text{U}_6\text{O}_4(\text{OH})_4(\text{H}_2\text{O})_2(2\text{-FA})_{12}]\cdot 8.76(\text{H}_2\text{O})$, and $[\text{U}_{38}\text{Cl}_{42}\text{O}_{56}(\text{H}_2\text{O})_{20}]\cdot m(\text{H}_2\text{O})\cdot n(\text{THF})$ (2-FA = 2-furoic acid, THF = tetrahydrofuran). The U^{IV} -oxo-clusters were tetranuclear $[\text{U}_4(\mu_3\text{O})_2\text{Cl}_4]$, two hexanuclear $\{\text{U}_6\text{O}_4(\text{OH})_4\}$, and a mixed-valence $\{\text{U}_{38}\}$ cluster (Fig. 23a). A similar $\{\text{U}_{38}\}$ cluster was first reported by Loiseau with the formula of $[\text{U}_{38}\text{O}_{56}\text{Cl}_{18}(\text{THF})_8(\text{bz})_{24}\cdot 8\text{THF}$ (Hzb = benzoic acid) in 2013 (Fig. 23b).¹³⁴ This kind of $\{\text{U}_{38}\}$ cluster could be viewed as a derivative of a face-centered cubic $\{\text{U}_{14}\}$ cluster. Six tetranuclear $\{\text{U}_4\}$ clusters combined with the six faces of $\{\text{U}_{14}\}$ to form the $\{\text{U}_{38}\}$ cluster. But it should be noted that there were no additional organic ligands in $[\text{U}_{38}\text{Cl}_{42}\text{O}_{56}(\text{H}_2\text{O})_{20}]\cdot[\text{U}_{38}\text{Cl}_{42}\text{O}_{56}(\text{H}_2\text{O})_{20}]$ was stabilized by bridging Cl ions and water molecules and was a pure inorganic cluster, while $[\text{U}_{38}\text{O}_{56}\text{Cl}_{18}(\text{THF})_8(\text{bz})_{24}]$ was stabilized by the coordination of terminal benzoic acid and THF ligands. Loiseau also synthesized a similar $\{\text{U}_{38}\}$ cluster with the formula $[\text{U}_{38}\text{O}_{56}\text{Cl}_{40}(\text{H}_2\text{O})_2(\text{ipa})_{20}]\cdot(\text{ipa})_x$ (ipa = isopropanol) in 2018 (Fig. 23c),¹³⁵ but the terminal ligands were ionized isopropanol molecules. In 2019, Mazzanti also reported a series of U^{IV} -oxo-clusters with multiple U-framework structures, including planiform $[\text{U}_6\text{O}_4(\text{PhCOO})_{16}(\text{Py})_4]$, fusiform $[\text{U}_{13}\text{K}_4\text{O}_{12}(\text{OH})_4(\text{PhCOO})_{12}\text{Cl}_{14}]\text{Cl}_2$ and $[\text{U}_{13}\text{K}_2\text{O}_9(\text{OH})_7(\text{PhCOO})_{12}\text{Cl}_{16}]\text{Cl}$, heart-like $[\text{U}_{16}\text{O}_{15}(\text{OH})_8(\text{PhCOO})_{26}(\text{Py})_2]$, oblate spheroidal $[\text{U}_{24}\text{O}_{30}(\text{OH})_2(\text{PhCOO})_{30}(\text{Py})_4\text{Cl}_4]$ and cubic $[\text{U}_{38}\text{O}_{56}\text{Cl}_{18}(\text{PhCOO})_{22}(\text{CH}_3\text{CONH}_2)_{10}]$.¹³⁶ Significantly, this $\{\text{U}_{38}\}$ cluster also exhibits a similar structure to the above three $\{\text{U}_{38}\}$ clusters (Fig. 23d).

To investigate the kinetic formation of the $\{\text{U}_{38}\}$ cluster, Loiseau studied the evolution of the products of this solvothermal reaction over time and found a new cationic $\{\text{U}_{12}\}$ cluster, $[\text{U}_{12}\text{O}_7(\text{OH})_4\text{Cl}_9(\text{H}_2\text{O})_9(\text{bz})_6(\text{gly})_6(\text{ox})_3]^{3+}$ (Hzb = benzoic acid, gly = glycolate, ox = oxalate), with a quadrahedron configuration (Fig. 24a and b).¹³⁷ Glycolate and oxalate were *in situ*

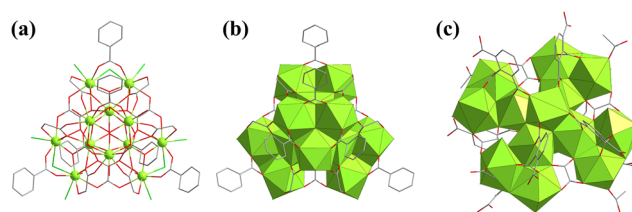


Fig. 24 (a) Ball-and-stick and (b) polyhedral views of $[\text{U}_{12}\text{O}_7(\text{OH})_4\text{Cl}_9(\text{H}_2\text{O})_9(\text{bz})_6(\text{gly})_6(\text{ox})_3]^{3+}$; (c) view of $[\text{U}_{14}\text{O}_8(\text{OH})_4\text{Cl}_8(\text{H}_2\text{O})_{16}(1,2,3\text{-Hbtc})_8(\text{ox})_4(\text{ac})_4]$. Color codes are the same as in Fig. 20.

formed from THF and benzoic acid. This $\{\text{U}_{12}\}$ cluster could be viewed as a derivative of $\{\text{U}_6\text{O}_4(\text{OH})_4\}$ combining three binuclear uranium clusters at three adjacent positions of $\{\text{U}_6\text{O}_4(\text{OH})_4\}$. All the uranium atoms in $\{\text{U}_{12}\}$ are in the +4 valence state. Additional $[(\text{U}^{\text{VI}}\text{O}_2)\text{Cl}_4]^{2-}$ balanced the charge. Subsequently, Loiseau also synthesized a $\{\text{U}_{14}\}$ cluster with the formula $[\text{U}_{14}\text{O}_8(\text{OH})_4\text{Cl}_8(\text{H}_2\text{O})_{16}(1,2,3\text{-Hbtc})_8(\text{ox})_4(\text{ac})_4]$ (1,2,3-H₃btc = benzene-1,2,3-tricarboxylic acid) (Fig. 24c).¹²⁵ This $\{\text{U}_{14}\}$ cluster could also be viewed as a derivative of $\{\text{U}_6\text{O}_4(\text{OH})_4\}$, which combined four groups of binuclear uranium clusters at the four equatorial positions of $\{\text{U}_6\text{O}_4(\text{OH})_4\}$.

In 2021, Ikeda-Ohno and co-workers synthesized a rare Keggin-type $\{\text{U}_{13}\}$ cluster, $[\text{U}_{13}(\text{CH}_3\text{O})_{35.7}\text{Cl}_{2.3}\text{O}_8]$, with mixed-valence U^{IV} and U^{V} (Fig. 25).¹³⁸ This compound was synthesized from a solution of methanol with $[\text{U}^{\text{IV}}\text{Cl}(\text{S})\text{-}(\text{PEBA})_3]$ ((S)-PEBA = (S,S)-N,N'-bis(1-phenylethyl)benzamidinate) or $[\text{U}^{\text{IV}}\text{Cl}_2(\text{salen})_2(\text{MeOH})_2]$ (H₂salen = N,N'-bis(salicylidene)ethylenediamine). Single-crystal structure and BVS results revealed that the valence state of the central uranium atom in $\{\text{U}_{13}\}$ was +5 and the other 12 uranium atoms were in the +4 valence state. Ionized MeOH acted as bridging and terminal ligands to stabilize this Keggin framework. Substitutionally disordered Cl ions occupied the equatorial position. This $\{\text{U}_{13}\}$ cluster is the first U-based Keggin-type cluster, which broadens the range of POMs.

At the beginning of 2021, Wang's group reported a tabular mixed-valence enneanuclear uranium cluster, $[\text{H}_3\text{O}^+][\text{U}^{\text{V}}(\text{U}^{\text{VI}}\text{O}_2)_8(\mu_3\text{O})_6(\text{PhCOO})_2(\text{Py}(\text{CH}_2\text{O})_2)_4(\text{DMF})_4]$ (Ph = phenyl, Py = pyridyl, DMF = *N,N*-dimethylformamide), which was dexterously synthesized from a mixed solution of DMF,

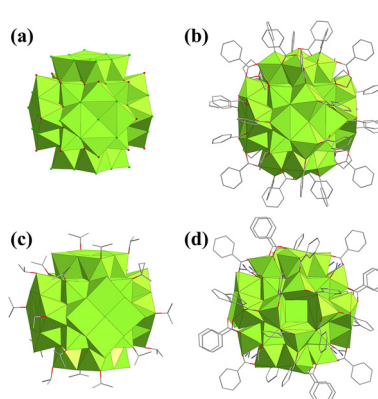


Fig. 23 Views of (a) $[\text{U}_{38}\text{Cl}_{42}\text{O}_{56}(\text{H}_2\text{O})_{20}]$, (b) $[\text{U}_{38}\text{O}_{56}\text{Cl}_{18}(\text{THF})_8(\text{bz})_{24}]$, (c) $[\text{U}_{38}\text{O}_{56}\text{Cl}_{40}(\text{H}_2\text{O})_2(\text{ipa})_{20}]$, and (d) $[\text{U}_{38}\text{O}_{56}\text{Cl}_{18}(\text{PhCOO})_{22}(\text{CH}_3\text{CONH}_2)_{10}]$. Color codes are the same as in Fig. 20.

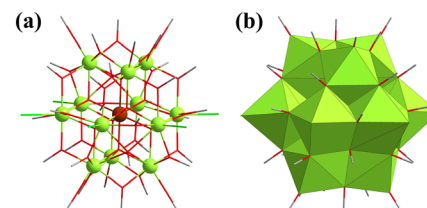
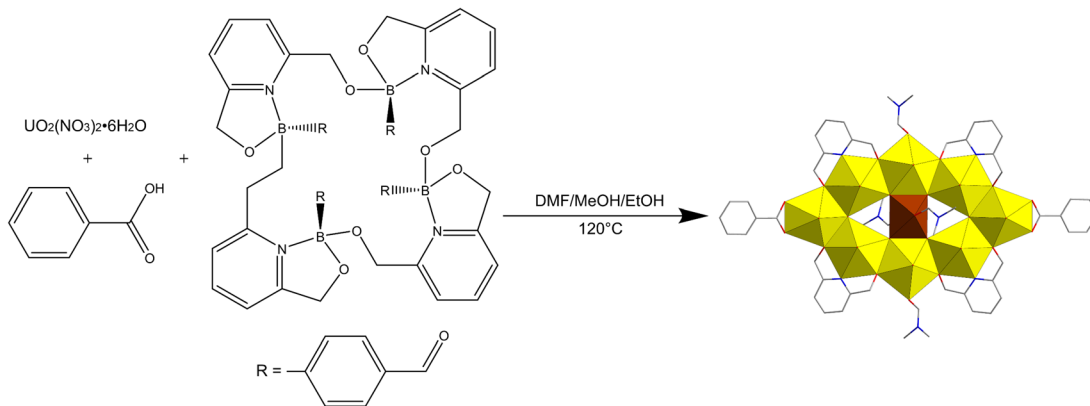


Fig. 25 (a) Ball-and-stick and (b) polyhedral views of $[\text{U}_{13}(\text{CH}_3\text{O})_{35.7}\text{Cl}_{2.3}\text{O}_8]$. Color codes are the same as in Fig. 21.



Scheme 1 Schematic diagram of the synthesis and structure of $[\text{H}_3\text{O}^+]\text{U}^{\text{V}}(\text{U}^{\text{VI}}\text{O}_2)_8(\mu_3\text{-O})_6(\text{PhCOO})_2(\text{Py}(\text{CH}_2\text{O})_2)_4(\text{DMF})_4$. Color codes are the same as in Fig. 21.

methanol, and ethanol with $\text{UO}_2(\text{NO}_3)_2 \cdot 6\text{H}_2\text{O}$, macrocyclic oligoboronate, and benzoic acid (Scheme 1).¹³⁹ The tetrameric borates *in situ* transformed into ionized pyridine-2,6-diyldimethanol ligands under solvothermal conditions, which might be the crucial factor for this synthesis. The central uranium ion was in an octahedral geometry and the valence was demonstrated to be +5 by various means. Density functional theory (DFT) and electronic spectroscopy revealed the outstanding semiconductor property of $[\text{H}_3\text{O}^+]\text{U}^{\text{V}}(\text{U}^{\text{VI}}\text{O}_2)_8(\mu_3\text{-O})_6(\text{PhCOO})_2(\text{Py}(\text{CH}_2\text{O})_2)_4(\text{DMF})_4$.

2.3 Other types of U-POMs

In addition to the above types of U-POMs, there are also other structures that are hard to classify as above. Due to the unique bonding law of uranium, fewer U-oxo-clusters are built from typical building units of POMs. Uranyl peroxide clusters and their derivatives are the most common compounds to be seen. There were several Lindqvist-type U-POMs in the early stage.^{12,140} In 2001, Clark and co-workers synthesized the first Lindqvist-type uranium cluster with crystal structures, *i.e.*, $[\text{Cp}_4(\text{bpy})_2]\text{[U}_6\text{O}_{13}]$ ($\text{Cp} = 1,2,4\text{-}t\text{Bu}_3\text{C}_5\text{H}_2$, bpy = 2,2-bipyridine), which was stabilized by the coordination of two kinds of aromatic ligands (Fig. 26).¹⁴¹ The average valence of U atoms should be +5 in consideration of charge balance and magnetic susceptibility. Then, Burns reported a non-normal wheel-shaped POM, $\{\text{[W}_5\text{O}_{21}]\}_3\text{[(U}^{\text{VI}}\text{O}_2)_2(\mu\text{-O}_2)]_3\}^{30-}$, in 2012 (Fig. 27).¹⁴² This compound was synthesized from a basic solu-

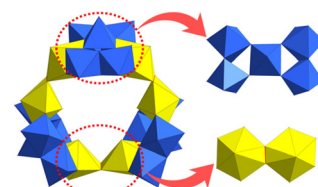


Fig. 27 View of $\{\text{[W}_5\text{O}_{21}]\}_3\text{[(U}^{\text{VI}}\text{O}_2)_2(\mu\text{-O}_2)]_3\}^{30-}$. Color codes are the same as in Fig. 1.

tion of $\text{UO}_2(\text{NO}_3)_2$, H_2O_2 , LiOH , NaOH , and $\text{H}_3\text{PW}_{12}\text{O}_{40}$. Being different from monovacant Lindqvist- $\{\text{W}_5\}$, the $\{\text{W}_5\}$ units in $\{\text{[W}_5\text{O}_{21}]\}_3\text{[(U}^{\text{VI}}\text{O}_2)_2(\mu\text{-O}_2)]_3\}^{30-}$ were in a planar configuration and the central W atom was in a tetragonal pyramid geometry. Six uranyl groups were connected by bridging- O_2^{2-} two by two. Three $\{\text{W}_5\}$ and three binuclear uranium clusters were linked alternately to form a triangular arrangement.

Although a series of Silverton-type U-containing polyoxomolybdates (U-POMOs) were reported very early, there were still no other types of U-POMOs until Nyman reported a U-POMO, *i.e.*, $5\text{Na}[\text{UNA}(\text{Mo}_6\text{P}_4\text{O}_{31}\text{H}_7)_2]\text{·}(\text{H}_2\text{O})_n$.¹⁴³ But there are no typical U-O-Mo bonds in this compound; this is one of the features of traditional POMs. The U^{4+} cations are linked by Anderson-like $\{\text{Mo}_6\}$ moieties through the connection of PO_4^{3-} . This is also the first U-POMO, except for the Silverton-type structures mentioned above.

Furthermore, Nyman also synthesized two Lindqvist-type U-containing polyoxoniobates (U-PONbs), *i.e.*, $[(\text{UO}_2)(\text{H}_2\text{O})_3\text{Nb}_{46}(\text{UO}_2)_2\text{O}_{136}\text{H}_8(\text{H}_2\text{O})_4]^{24-}$ and $[(\text{Nb}_{22}\text{H}_2)_4(\text{UO}_2)_7(\text{H}_2\text{O})_6]^{22-}$; these are also currently the only two U-PONbs (Fig. 28).¹⁴⁴ However, there is significant disorder of uranyl ions in both structures. The structure of $[(\text{UO}_2)(\text{H}_2\text{O})_3\text{Nb}_{46}(\text{UO}_2)_2\text{O}_{136}\text{H}_8(\text{H}_2\text{O})_4]^{24-}$ could be divided into two parts, namely three ordered uranyl ions as linkers and two groups of $\{\text{Nb}_7\}$ triquetrous trimers linked by $\{\text{NbO}_2\}$ or disordered $\{\text{UO}_2\}$. For the other U-PONbs, two of the three kinds of uranyl ions exhibit positional disorder around a center of symmetry in $[(\text{Nb}_{22}\text{H}_2)_4(\text{UO}_2)_7(\text{H}_2\text{O})_6]^{22-}$. The occupancies

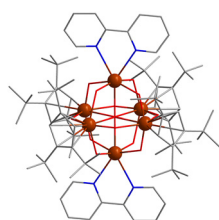


Fig. 26 View of $[\text{Cp}_4(\text{bpy})_2]\text{[U}_6\text{O}_{13}]$. Color codes are the same as in Fig. 21.

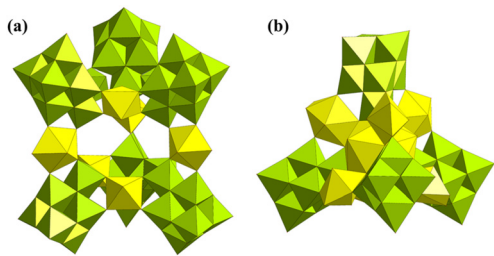


Fig. 28 Views of (a) $[(\text{UO}_2)(\text{H}_2\text{O})_3\text{Nb}_{46}(\text{UO}_2)_2\text{O}_{136}\text{H}_8(\text{H}_2\text{O})_4]^{24-}$ and (b) $[(\text{Nb}_7\text{O}_{22}\text{H}_2)_4(\text{UO}_2)_7(\text{H}_2\text{O})_6]^{22-}$. Color codes are the same as in Fig. 1; Nb, lime.

of U2 and U3 are 0.5 and 0.25, respectively. Each $\{\text{Nb}_7\}$ cluster is connected with two U1, one U2, and three U3 to form a symmetric tetrahedral sandwich structure. These two U-PONbs were synthesized by a similar vapour diffusion method from EtOH diffusing into a solution containing $\text{TMA}_6[\text{Nb}_{10}\text{O}_{28}]$ and $\text{Li}_4[\text{UO}_2(\text{O}_2)_3]$. The utilization of these two raw materials instead of the normal K salt of $\{\text{Nb}_{10}\}$ and $\text{UO}_2(\text{NO}_3)_2$ may be the significant factor for the construction of the only two U-PONbs.

Besides, there is a type of uranium hydroxide cluster outside the above classification, which might be more appropriately called inorganic uranium mineral compounds, but their single-crystal structures are rarely reported.¹³ Recently, a new uranium oxide hydrate with a 3D framework was obtained by Zhang and co-workers. $[\text{U}(\text{H}_2\text{O})_2]\{[(\text{UO}_2)_{10}\text{O}_{10}(\text{OH})_2][(\text{UO}_4)(\text{H}_2\text{O})_2]\}$ was hydrothermally synthesized from schoepite at high temperature (240 °C) (Fig. 29).¹⁴⁵ Single-crystal structure, BVS, and other characterization methods demonstrated the presence of mixed-valence U^{IV} and U^{VI} .

3. Characterization, properties, and applications

Early research on U-POMs may be limited by research conditions and only spectroscopy and electrochemistry investigations were carried out for most of the U-POMs.¹⁴⁶ X-ray single-crystal diffraction came into service at the end of the 20th century.^{30,63,140} In addition to X-ray single-crystal diffraction, basic spectroscopy investigations were carried out for most of the U-POMs, including FT-IR, Raman, UV/vis, elec-

tronic spectra and so on.⁶⁵⁻⁶⁷ Nuclear magnetic resonance (NMR) spectroscopy of characteristic elements (P, W, *etc.*) was also utilized to study the structure and solution behaviors of some U-POMs.^{30,34,60} Magnetic properties were investigated for some U-POMs due to the paramagnetic nature of $\text{U}^{\text{IV}}/\text{U}^{\text{V}}$.^{68,133,139,141} Magnetic susceptibility tests could also verify the valence of uranium atoms. Other normal characterization methods such as TGA and PXRD were also investigated for several U-POMs. However, it should be noted that, maybe due to the strong absorption effects in X-ray diffraction, most of the reported PXRD results for U-POMs did not show diffraction peaks as clearly as those of other POMs.^{31,32} In recent years, small-angle X-ray scattering (SAXS) was used to investigate POMs in solution, especially uranyl peroxide clusters.¹⁴⁷ The sizes of POMs in solution could be revealed by the SAXS results and thus the free states of POMs in solution could be indicated. SAXS was also used to study the solution assembly and behavior of uranyl peroxide clusters.¹⁴⁸ Burns also used neutron diffraction to study the crystal structures of $\text{Na}_{44}\text{K}_6[(\text{UO}_2)_{24}(\text{O}_2)_{24}(\text{P}_2\text{O}_7)_{12}][\text{IO}_3]_2 \cdot 140\text{H}_2\text{O}$ and $\{\text{U}_{60}\}$, which revealed abundant structural information beyond that obtained from X-ray diffraction.^{149,150} In addition to BVS and X-ray photoelectron spectroscopy (XPS), X-ray absorption near edge structure (XANES) spectroscopy could also help to determine the valence of uranium atoms.¹³⁹ Besides, ESI-MS is a powerful way to study species in solution and understand the assembly of complicated molecules. Burns used Raman spectroscopy and ESI-MS to study the dissolution of UO_2 in a basic solution containing XOH ($\text{X} = \text{Li, Na, K}$) and H_2O_2 .¹⁵¹ This process was found to be linearly dependent on the concentrations of alkali, which could rival the usage of boiling HNO_3 . Several uranyl peroxide clusters were formed in this process. This work could help to control the dissolution and separation of UO_2 in solution. Finally, density functional theory (DFT) calculations could also help people to learn the structure of several U-POMs.^{139,142,152} Perhaps the vacuum conditions of the scanning electron microscope (SEM) and transmission electron microscope (TEM) make solvent-rich U-POM crystals decompose easily; SEM and TEM technology are occasionally used to observe U-POMs.^{132,133,137,153-155}

In terms of properties and applications, only a few investigations were carried out in addition to magnetic studies. Firstly, early research revealed that the study of U-POWs could help people to dispose of radioactive elements because POws exhibited outstanding thermal stability and radioresistance. Those obtained U-POWs may benefit the development of the immobilization, enrichment, and separation of radionuclides.^{30,146,156,157} The residue of U-POWs after high-temperature calcination could result in uranium-containing tungsten bronzes, which may provide a direction for handling radioactive materials.¹⁵⁸

Secondly, due to the luminescent nature of uranyl ions, U-POMs may also exhibit good luminescence properties, but there were no studies on the luminescence properties of U-POMs until recently.^{41,49,62} In 2021, Kong's group systematically studied the temperature-dependent photoluminescence

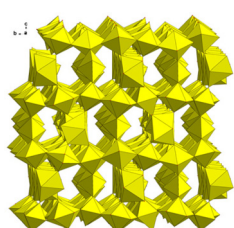


Fig. 29 View of $[\text{U}(\text{H}_2\text{O})_2]\{[(\text{UO}_2)_{10}\text{O}_{10}(\text{OH})_2][(\text{UO}_4)(\text{H}_2\text{O})_2]\}$. Color codes are the same as in Fig. 1.

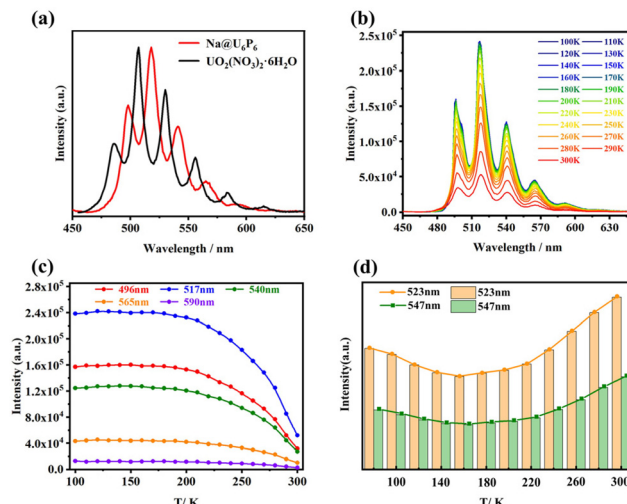
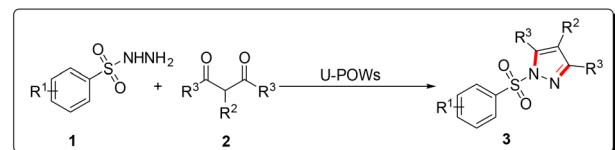


Fig. 30 (a) Solid-state photoluminescence emission spectra of $\text{Na@U}_6\text{P}_6$ and $\text{UO}_2(\text{NO}_3)_2 \cdot 6\text{H}_2\text{O}$ ($\lambda_{\text{ex}} = 441$ nm, normalized intensity); (b) emission map of spectra recorded from 100 to 300 K; variation trend of emission peaks depends on temperature for (c) $\text{Na@U}_6\text{P}_6$ and (d) U_3 . Reprinted with permission from ref. 41 and 62. Copyright 2021 American Chemical Society and 2022 Elsevier, respectively.

properties of $\text{Na}_{17}[\text{Na}@\{(\text{SbW}_9\text{O}_{33})_2(\text{UO}_2)_6(\text{PO}_3\text{OH})_6\}] \cdot x\text{H}_2\text{O}$ ($\text{Na@U}_6\text{P}_6$) for the first time (Fig. 30a–c).⁴¹ $\text{Na@U}_6\text{P}_6$ displayed a similar emission peak shape to that of $\text{UO}_2(\text{NO}_3)_2 \cdot 6\text{H}_2\text{O}$. The solid-state photoluminescence quantum yield of $\text{Na@U}_6\text{P}_6$ is 33%. When the temperature increases from 100 to 300 K, $\text{Na@U}_6\text{P}_6$ shows a relatively stable emission from 100 to 200 K and then the emission intensity sharply decreases from 200 to 300 K. The dominant non-radiative transitions should be responsible for this phenomenon at high temperatures. Whereafter, our group and Zhang's group also studied the temperature-dependent properties of $\text{K}_{1.5}\text{Na}_{13.25}[(\text{UO}_2)_3(\text{SeO}_3)_3\text{Na}_5(\text{H}_2\text{O})_6(\text{SeW}_6\text{O}_{21})(\text{SeW}_9\text{O}_{33})_3] \cdot 26\text{H}_2\text{O}$ (U_3).⁶² While the solid-state photoluminescence quantum yield of U_3 is 72%. What is noteworthy is that $\text{Na@U}_6\text{P}_6$ and U_3 show different emission trends depending on temperature. U_3 undergoes a decrease and then increases with increasing temperature, which could result from changes in non-radiative decay and radiative decay (Fig. 30d). The temperature-dependent photoluminescence properties of $\text{Na@U}_6\text{P}_6$ and U_3 demonstrate that U-POMs have great potential as luminescent materials.

Thirdly, most U-hetero-POMs should retain the catalytic characteristics of POMs and uranium compounds. Thus, U-hetero-POMs could be used as bifunctional Lewis acid–base catalysts in organic synthesis. However, there were also no studies on the catalytic activities of U-hetero-POMs until recently. Our group synthesized six U-POWs to catalyze the synthesis of sulfonyl pyrazoles and/or 3H-benzo[b][1,4]diazepines, namely $\text{Na}_{11}\text{H}(\text{H}_2\text{O})_{31}[\text{Na}(\text{UO}_2)(\text{PW}_9\text{O}_{34})_2] \cdot 7\text{H}_2\text{O}$ ($\text{UPW}_9\text{-1}$), $\text{Na}_{12}(\text{H}_2\text{O})_{29}[\text{Na}(\text{UO}_2)(\text{PW}_9\text{O}_{34})_2] \cdot 7\text{H}_2\text{O}$ ($\text{UPW}_9\text{-2}$), $\text{Na}_{10.5}\text{H}_{3.5}(\text{H}_2\text{O})_{36}[\text{Na}(\text{UO}_2)(\alpha\text{-SiW}_9\text{O}_{34})_2] \cdot 2.5\text{H}_2\text{O}$ ($\text{USiW}_9\text{-1}$), $\text{Na}_{14}(\text{H}_2\text{O})_{36}[\text{Na}(\text{UO}_2)(\alpha\text{-SiW}_9\text{O}_{34})_2] \cdot 4\text{H}_2\text{O}$ ($\text{USiW}_9\text{-2}$), $(\text{Se}_2\text{U}_2)\text{Na}_3[\text{H}_{19}(\text{UO}_2)_2(\mu_2\text{-O})(\text{Se}_2\text{W}_{14}\text{O}_{52})_2] \cdot 41\text{H}_2\text{O}$ (U_2), and $(\text{NH}_4)_{10}[\text{H}_4(\text{SeO})_2]$.



Catalyst: $\text{UPW}_9\text{-1}$
Substrate 1: $\text{R}^1 = \text{H, 4-CH}_3, 4\text{-CH}_2\text{O, 4-Cl, 3-Cl, 2-Cl, 4-NO}_2$ and .
Substrate 2:
Reaction conditions: 1 (1 mol), 2 (1 mol), $\text{UPW}_9\text{-1}$ (1 mol%), EtOH (0.1 mL), 80–110 °C, 60–80 min
Yield: 91–99%

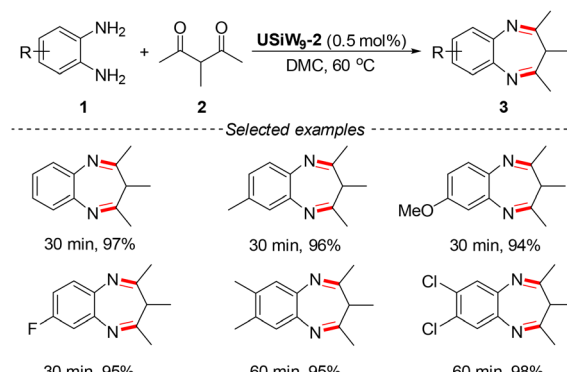
Catalyst: $\text{USiW}_9\text{-2}$
Substrate 1: $\text{R}^1 = \text{H}$
Substrate 2:
Reaction conditions: 1 (1 mol), 2 (1 mol), $\text{USiW}_9\text{-2}$ (0.5 mol%), DMC (0.1 mL), 60 °C, 1 h
Yield: 98–99%

Catalyst: U_2
Substrate 1: $\text{R}^1 = \text{H, 4-CH}_3, 4\text{-Cl}$
Substrate 2:
Reaction conditions: 1 (1 mol), 2 (1 mol), U_2 (0.2 mol%), solvent-free, 80 °C, 1 h
Yield: 93–99%

Scheme 2 Summary of the synthesis of sulfonyl pyrazoles catalyzed by $\text{UPW}_9\text{-1}$, $\text{USiW}_9\text{-2}$, and U_2 .

$(\text{UO}_2)_2(\text{H}_2\text{O})_2(\text{H}_2\text{Se}_2\text{W}_{14}\text{O}_{52})(\text{Se}_2\text{W}_{14}\text{O}_{52}) \cdot 66\text{H}_2\text{O}$ (Se_2U_2), which demonstrated the catalytic activities of U-POWs (Schemes 2 and 3).^{31,32} These catalytic systems showed advantages such as benign conditions, excellent yields, good compatibility, and atom efficiency.

Fourthly, U-oxo-clusters including uranyl peroxide clusters and other similar POMs are a broad category of compounds with a high density of uranium atoms. Therefore, the study of U-oxo-clusters may benefit the development of nuclear fuel cycle technologies and mixed oxide (MOX) nuclear fuel.^{159–163}



Scheme 3 Substrate scope for the synthesis of benzodiazepines catalyzed by $\text{USiW}_9\text{-2}$. Reaction conditions: diamines 1 (1 mmol), 2 (1 mmol), catalyst (0.5 mol%), DMC (0.1 mL) or solvent-free; isolated yields.

Besides, the ion-rich nature of uranyl peroxide clusters and other similar clusters make them good for ion storage. Yin's group recently synthesized a kind of hybrid nanocomposite for solid-state electrolytes using $\{U_{60}\}$ ($Li_{44}K_{16}[UO_2(O_2)(OH)]_{60}$) and cationic surfactants.¹⁶⁴ The cavity makes capsule-like $\{U_{60}\}$ a good storage and transportation node for Li^+ . Different surfactants could regulate the microphase-separated structures of the nanocomposites from lamellar to columnar structures. This work represents a new direction for the application of uranyl peroxide clusters.

Finally, Wang's work revealed the n-type semiconductor behavior of $[H_3O^+][U^V(U^{VI}O_2)_8(\mu_3-O)_6(PhCOO)_2(Py(CH_2O)_2)_4(DMF)_4]$.¹³⁹ Due to the unique tabular mixed-valence structure, the central U^V could act as an electron donor under X-ray radiation. $[H_3O^+][U^V(U^{VI}O_2)_8(\mu_3-O)_6(PhCOO)_2(Py(CH_2O)_2)_4(DMF)_4]$ could produce a photocurrent, which makes it a potential X-ray detecting semiconductor material. This work shows us the potential of U-oxo-cluster-based semiconductor materials due to the multivalent nature of uranium.

4. Summary and outlook

In summary, one could be aware that the development of U-POMs is still relatively slow despite the early study of U-POMs beginning in the 1990s. Most of the reported U-hetero-POMs and the two main categories of U-oxo-clusters were structure-driven studies. In contrast, the focus of research on mainstream POMs has developed from structure-driven research to performance-driven research. The current situation for U-POMs is that knowledge of the structural diversities and involved elements is still deficient, and the applications of U-POMs are still less explored even though there are dozens of U-POMs. In terms of numbers, although the number is relatively small, there are still dozens of U-hetero-POMs and uranyl hydroxide clusters. In contrast, U^{IV} -oxo-clusters are sporadically reported and the number is quite low. In terms of synthesis, the U-hetero-POMs are still less explored not only due to the difficulty in controlling the self-assembly process of POMs but also the limitations of the vacancy-directed synthetic strategy. Almost all the U-hetero-POMs are synthesized using polyvacant anionic precursors. There were fewer than ten cases of U-hetero-POMs *in situ* synthesized until recently. U-oxo-clusters reported in recent years have gradually developed from pure inorganic structures to organic-inorganic hybrid structures. However, the discovery of new topologies of uranyl peroxide clusters has gradually slowed down in recent years, which may be because of the limitations of applications due to the soluble nature of uranyl peroxide clusters and expensive costs of synthesis. Meanwhile, the much rarer U^{IV} -oxo-clusters are always synthesized using organic solvent and some ligands under solvothermal synthesis. But the organic ligands are still limited to organic phosphonic acids for uranyl peroxide clusters and a finite number of ligands for U^{IV} -oxo-clusters even if there are multiple changes to these ligands. Thus, the research prospects of U-POMs are still attractive.

From the viewpoint of synthesis and structures, research on U-POMs still exhibits great possibilities.

(i) First, most U-hetero-POMs are synthesized by a precursor approach from an aqueous solution at room temperature. There were fewer than ten cases synthesized from simple materials, *i.e.*, *in situ* methods. Thus, the utilization of *in situ* and hydrothermal methods may result in more unprecedented POMs with various structures.

(ii) Second, most of the U-POMs are pure inorganic compounds crystallized from an aqueous solution. Thus, these inorganic U-POMs may exhibit considerable solubility in polar solvents, which limits their application in some fields such as catalysis and the immobilization and enrichment of radionuclides. Referring to other POMs, especially lanthanide-containing POMs, the introduction of organic ligands may make the obtained U-POMs more insoluble and diverse. Interesting properties and applications may also be discovered related to these molecules. The study of organic-inorganic hybrid U-POMs may show more possibilities and expansive prospects.

(iii) Third, the synthesized U-hetero-POMs for now mainly focus on POWs, but other POMs are rarely involved, such as Mo, V, Nb, and Ta. Thus, it should be recognized that the study of U-POMs lags far behind other POMs, which may be limited by the synthesis method. More synthesis strategies could be applied according to other POMs. More synthesis methodologies should be introduced by referring to the synthesis of metal-organic frameworks. Synthesis strategies such as hydrothermal, solvothermal, ionothermal, microwave, ultrasonic, mechanochemical, and *in situ* ligand reactions should be applied more, especially for U-oxo-clusters.

(iv) Fourth, due to the unique bonding nature of uranium atoms, the formation of uranyl peroxide clusters and metal-organic U-oxo-clusters is more common, but typical types of POMs (Keggin, Lindqvist, *etc.*) are hard to see. Thus, the synthesis of U-oxo-clusters with typical types of POMs still faces challenges and risks. For solvothermally synthesized U^{IV} -oxo-clusters, the introduction of more different kinds of ligands into U-oxo-clusters could result in unpredictable changes and may help to broaden the scope of U-POMs.

From the perspective of applications, research on most of the U-POMs was only based on the characterizations of the structures by spectroscopic methods. Only a few studies on U-POMs have addressed applications such as magnetism, catalysis, temperature-dependent fluorescence, and the immobilization and enrichment of radionuclides. Thus, performance-oriented research on U-POMs requires more work. Firstly, only a few cases of magnetism studies of low valent U-POMs revealed their potential as magnetic materials such as single-molecular magnets. But this research is all superficial and deeper investigations are needed with reference to lanthanide-containing POMs. Secondly, Kong's and our work demonstrated the U-POMs' luminescence ability. U-POMs may exhibit good potential as luminescent materials such as probes and imaging agents, as well as for application in radioactive medicine.^{41,62} Thirdly, our work revealed the thermocatalytic activities of U-POWs for the synthesis of N-heterocyclic com-

pounds, and more catalytic systems should be explored.^{30,31} Fourthly, the application in solid-state electrolytes and ion transport for ion-rich uranyl peroxide clusters is also a direction for traditional U-oxo-clusters.¹⁶⁴ Fifthly, for those mixed-valence U-oxo-clusters, the inner charge-transfer property makes them potential semiconductor materials.¹³⁹ Thus, semiconductor-related applications may be another remarkable direction for those U-oxo-clusters, such as photoelectric conversion, sensors, devices, and so on. Finally, considering the optical nature of uranium and uranyl compounds and the catalytic advantages of POMs, the application of photocatalysis may be an attractive outlet for U-POMs, especially for those mixed-valence uranium-containing U-POMs. U-POMs may show great potential in the field of photocatalysis, including photocatalytic organic synthesis, photocatalytic degradation of pollutants, photocatalytic hydrogen production, and so on.

Conflicts of interest

There are no conflicts to declare.

Acknowledgements

This work was financially supported by the National Natural Science Foundation of China (22001034), the Open Fund of the Jiangxi Province Key Laboratory of Synthetic Chemistry (JXSC202008), and the Research Fund of East China University of Technology (DHBK2019264).

References

- 1 H. N. Miras, J. Yan, D. L. Long and L. Cronin, Engineering polyoxometalates with emergent properties, *Chem. Soc. Rev.*, 2012, **41**, 7403–7430.
- 2 W. W. He, S. L. Li, H. Y. Zang, G. S. Yang, S. R. Zhang, Z. M. Su and Y. Q. Lan, Entangled structures in polyoxometalate-based coordination polymers, *Coord. Chem. Rev.*, 2014, **279**, 141–160.
- 3 D. Y. Du, J. S. Qin, S. L. Li, Z. M. Su and Y. Q. Lan, Recent advances in porous polyoxometalate-based metal–organic framework materials, *Chem. Soc. Rev.*, 2014, **43**, 4615–4632.
- 4 M. Taghizadeh, E. Mehrvarz and A. Taghipour, Polyoxometalate as an effective catalyst for the oxidative desulfurization of liquid fuels: a critical review, *Rev. Chem. Eng.*, 2020, **36**, 831–858.
- 5 V. Das, R. Kaushik and F. Hussain, Heterometallic 3d-4f polyoxometalates: An emerging field with structural diversity to multiple applications, *Coord. Chem. Rev.*, 2020, **413**, 213271.
- 6 A. Misra, K. Kozma, C. Streb and M. Nyman, Beyond charge balance: Counter-cations in polyoxometalate chemistry, *Angew. Chem., Int. Ed.*, 2020, **59**, 596–612.
- 7 Y. Liu, C. S. Tang, M. Cheng, M. Chen, S. Chen, L. Lei, Y. S. Chen, H. Yi, Y. K. Fu and L. Li, Polyoxometalate@metal–organic framework composites as effective photocatalysts, *ACS Catal.*, 2021, **11**, 13374–13396.
- 8 B. D'Cruz, M. O. Amin and E. Al-Hetlani, Polyoxometalate-based materials for the removal of contaminants from wastewater: A review, *Ind. Eng. Chem. Res.*, 2021, **60**, 10960–10977.
- 9 P. Baidala, V. S. Smurova, E. A. Torchennkova and V. I. Spitsyn, Heteropoly molybdouranic acid and its ammonium salt, *Dokl. Chem.*, 1971, **197**, 202.
- 10 J. Qiu and P. C. Burns, Clusters of actinides with oxide, peroxide, or hydroxide bridges, *Chem. Rev.*, 2013, **113**, 1097–1120.
- 11 T. Auvray and E. M. Matson, Polyoxometalate-based complexes as ligands for the study of actinide chemistry, *Dalton Trans.*, 2020, **49**, 13917–13927.
- 12 M. Dufaye, S. Duval and T. Loiseau, Trends and new directions in the crystal chemistry of actinide oxo-clusters incorporated in polyoxometalates, *CrystEngComm*, 2020, **22**, 3549–3562.
- 13 P. C. Burns, in *Structural Chemistry of Inorganic Actinide Compounds*, Elsevier, 2007, ch. 1, pp. 1–30.
- 14 S. V. Krivovichev, P. C. Burns, I. G. Tananaev and B. F. Myasoedov, in *Structural Chemistry of Inorganic Actinide Compounds*, Elsevier, 2007, ch. 12, pp. 443–456.
- 15 M. T. Pope, in *Structural Chemistry of Inorganic Actinide Compounds*, Elsevier, 2007, ch. 9, pp. 341–361.
- 16 V. I. Spitsyn, Some features of actinide chemistry, *Radiokhimiya*, 1985, **27**, 241–254.
- 17 A. B. Yusov and V. P. Shilov, Complexes of f elements with heteropolyanions, *Radiochemistry*, 1999, **41**, 1–23.
- 18 K. E. Knope and L. Soderholm, Solution and solid-state structural chemistry of actinide hydrates and their hydrolysis and condensation products, *Chem. Rev.*, 2013, **113**, 944–994.
- 19 M. R. MacDonald, M. E. Fieser, J. E. Bates, J. W. Ziller, F. Furche and W. J. Evans, Identification of the +2 oxidation state for uranium in a crystalline molecular complex, $[K(2.2.2-Cryptand)]\llbracket(C_5H_4SiMe_3)_3U\rrbracket$, *J. Am. Chem. Soc.*, 2013, **135**, 13310–13313.
- 20 J. Selbin and J. D. Ortego, Chemistry of uranium(v), *Chem. Rev.*, 1969, **69**, 657–671.
- 21 I. Grenthe, J. Drozdynski, T. Fujino, E. C. Buck, T. E. Albrecht-Schmitt and S. F. Wolf, in *The Chemistry of the Actinide and Transactinide Elements*, Springer, 2008, vol. 1, ch. 5, pp. 253–698.
- 22 T. Loiseau, I. Mihalcea, N. Henry and C. Volkringer, The crystal chemistry of uranium carboxylates, *Coord. Chem. Rev.*, 2014, **266**, 69–109.
- 23 S. T. Liddle, The renaissance of non-aqueous uranium chemistry, *Angew. Chem., Int. Ed.*, 2015, **54**, 8604–8641.
- 24 M. Mazzanti, R. Faizova, F. Fadaei-Tirani and A. S. Chauvin, Synthesis and characterization of water stable uranyl(V) complexes, *Angew. Chem., Int. Ed.*, 2021, **60**, 8227–8235.

25 E. A. Dolgopolova, O. A. Ejegbawwo, C. R. Martin, M. D. Smith, W. Setyawan, S. Karakalos, C. H. Henager, H.-C. Z. Loya and N. B. Shustova, Multifaceted modularity: a key for stepwise building of hierarchical complexity in An-MOFs, *J. Am. Chem. Soc.*, 2017, **139**, 16852–16861.

26 O. A. Ejegbawwo, C. R. Martin, O. A. Olorunfemi, G. A. Leith, R. T. Ly, A. M. Rice, E. A. Dolgopolova, M. D. Smith, S. G. Karakalos, N. Birkner, B. A. Powell, S. Pandey, R. J. Koch, S. T. Misture, H.-C. Z. Loya, S. R. Phillipot, K. S. Brinkman and N. B. Shustova, Thermodynamics and electronic properties of heterometallic multinuclear actinide-containing metal–organic frameworks with “structural memory”, *J. Am. Chem. Soc.*, 2019, **141**, 11628–11640.

27 C. Falaise, C. Volkringer, J. F. Vigier, N. Henry, A. Beaurain and T. Loiseau, Three-dimensional MOF-type architectures with tetravalent uranium hexanuclear motifs (U_6O_8), *Chem. – Eur. J.*, 2013, **19**, 5324–5331.

28 S. Duval, S. Beghin, C. Falaise, X. Trivelli, P. Rabu and T. Loiseau, Stabilization of tetravalent 4f (Ce), 5d (Hf), or 5f (Th, U) clusters by the $[\alpha\text{-SiW}_9O_{34}]^{10-}$ polyoxometalate, *Inorg. Chem.*, 2015, **54**, 8271–8280.

29 C. M. Tourné, G. F. Tourné and M.-C. Briano, Bis(undecatungstogermanato)uranate(IV) de Césium: $Cs_{12}[U(GeW_{11}O_{39})_2] \cdot 13\text{--}14H_2O$, *Acta Crystallogr., Sect. B: Struct. Crystallogr. Cryst. Chem.*, 1980, **36**, 2012–2018.

30 K.-C. Kim and M. T. Pope, Cation-directed structure changes in polyoxometalate chemistry. Equilibria between isomers of bis(9-tungstophosphatodioxouranate(VI)) complexes, *J. Am. Chem. Soc.*, 1999, **121**, 8512–8517.

31 G. P. Yang, X. L. Zhang, Y. F. Liu, D. D. Zhang, K. Li and C. W. Hu, Self-assembly of Keggin-type U(vi)-containing tungstophosphates with a sandwich structure: an efficient catalyst for the synthesis of sulfonyl pyrazoles, *Inorg. Chem. Front.*, 2021, **8**, 4650–4656.

32 J. Zhou, T. Yu, K. Li, K. Zeng, G. P. Yang and C. W. Hu, Two U(vi)-containing silicotungstates with sandwich structures: lewis acid–base synergistic catalyzed synthesis of benzodiazepines and pyrazoles, *Inorg. Chem.*, 2022, **61**, 3050–3057.

33 K. Li, X. L. Lin, K. Zeng, X. F. Gao, W. Cen, Y. F. Liu and G. P. Yang, Effect of $Na(i)\text{-H}_2O$ clusters on self-assembly of sandwich-type U(vi)-containing silicotungstates and the efficient catalytic activity for the synthesis of substituted phenylsulfonyl-1H-pyrazoles, *Tungsten*, 2022, **4**, 149–157.

34 K.-C. Kim, A. Gaunt and M. T. Pope, New heteropolytungstates incorporating dioxouranium(vi). Derivatives of $\alpha\text{-}[SiW}_9O_{34}]^{10-}$, $\alpha\text{-}[AsW}_9O_{33}]^{9-}$, $\gamma\text{-}[SiW}_{10}O_{36}]^{8-}$, and $[As_4W_{40}O_{140}]^{28-}$, *J. Cluster Sci.*, 2002, **13**, 423–436.

35 A. J. Gaunt, I. May, R. Coping, A. I. Bhatt, D. Collison, O. D. Fox, K. T. Holman and M. T. Pope, A new structural family of heteropolytungstate lacunary complexes with the uranyl, UO_2^{2+} , cation, *Dalton Trans.*, 2003, 3009–3014.

36 R. Khoshnavazi, H. Eshtiagh-Hossieni, M. H. Alizadeh and M. T. Pope, Syntheses and structures determination of new polytungstoarsenates $[Na_2As_2W_{18}U_2O_{72}]^{12-}$ and $[MAS_2W_{18}U_2O_{72}]^{13-}$ ($M=NH_4^+$ and K^+), *Polyhedron*, 2006, **25**, 1921–1926.

37 R. X. Tan, X. H. Wang, F. Chai and Z. M. Su, Polyoxotungstates containing uranyl group: Germanotungstates with Keggin sandwich structure, *Inorg. Chem. Commun.*, 2006, **9**, 1331–1334.

38 M. H. Alizadeh and M. Mohadeszadeh, Sandwich-type uranium-substituted of bismuthotungstate: synthesis and structure determination of $[Na(UO_2)_2(H_2O)_4(BiW_9O_{33})_2]^{13-}$, *J. Cluster Sci.*, 2008, **19**, 435–443.

39 M. Mohadeszadeh, A supramolecular star-like tungstoarsenate(V) with uranyl cations: $[(NH_4)_{12}(UO_2(H_2O))_6(UO_2(\mu_2-H_2O))_6(\alpha\text{-AsW}_9O_{34})_6]^{18-}$, *J. Cluster Sci.*, 2011, **22**, 183–192.

40 S. Duval, S. Sobanska, P. Roussel and T. Loiseau, $B\text{-}\alpha\text{-}[AsW}_9O_{33}]^{9-}$ polyoxometalates incorporating hexanuclear uranium $\{U_6O_8\}$ -like clusters bearing the U^{IV} form or unprecedented mixed valence U^{IV}/U^{VI} involving direct $U^{VI}=O\text{-}U^{IV}$ bonding, *Dalton Trans.*, 2015, **44**, 19772–19776.

41 H. Y. Wang, X. Y. Zheng, L. S. Long, X. J. Kong and L. S. Zheng, Sandwich-type uranyl phosphate–polyoxometalate cluster exhibiting strong luminescence, *Inorg. Chem.*, 2021, **60**, 6790–6795.

42 A. J. Gaunt, I. May, D. Collison, K. T. Holman and M. T. Pope, Polyoxometal cations within polyoxometalate anions. Seven-coordinate uranium and zirconium heteroatom groups in $[(UO_2)_{12}(\mu_3\text{-O})_4(\mu_2\text{-H}_2O)_{12}(P_2W_{15}O_{56})_4]^{32-}$ and $[Zr_4(\mu_3\text{-O})_2(\mu_2\text{-OH})_2(H_2O)_4(P_2W_{16}O_{59})_2]^{14-}$, *J. Mol. Struct.*, 2003, **656**, 101–106.

43 M. H. Chiang, C. W. Williams, L. Soderholm and M. R. Antonio, Coordination of actinide ions in Wells–Dawson heteropolyoxoanion complexes, *Eur. J. Inorg. Chem.*, 2003, **2003**, 2663–2669.

44 A. Ostuni, R. E. Bachman and M. T. Pope, Multiple diastereomers of $[M^{n+}(\alpha_m\text{-P}_2W_{17}O_{61})_2]^{(20-n)-}$ ($M=U^{IV}$, ThIV, CeIII; $m=1, 2$). Syn-and anti-conformations of the polytungstate ligands in $\alpha_1\alpha_1$, $\alpha_1\alpha_2$, and $\alpha_2\alpha_2$ complexes, *J. Cluster Sci.*, 2003, **14**, 431–446.

45 M. N. Sokolova, A. M. Fedossev, G. B. Andreev, N. A. Budantseva, A. B. Yusov and P. Moisy, Synthesis and structural examination of complexes of Am(iv) and other tetravalent actinides with lacunary heteropolyanion $\alpha_2\text{-P}_2W_{17}O_{61}]^{10-}$, *Inorg. Chem.*, 2009, **48**, 9185–9190.

46 Y. G. Chen, F. X. Meng, H. J. Pang, D. M. Shi and Y. Sun, A novel uranyl complex with dimeric lacunary polyoxoanion: $[(A\text{-}\alpha\text{-SiW}_9O_{33})_2K\{UO_2(H_2O)\}_2]^{11-}$, *J. Cluster Sci.*, 2007, **18**, 396–405.

47 S. S. Mal, M. H. Dickman and U. Kortz, Actinide polyoxometalates: incorporation of uranyl–peroxo in U-shaped 36–tungsto–8–phosphate, *Chem. – Eur. J.*, 2008, **14**, 9851–9855.

48 M. Dufaye, S. Duval, G. Stoclet, X. Trivelli, M. Huve, A. Moissette and T. Loiseau, Uranyl cation incorporation in the $[P_8W_{48}O_{184}]^{40-}$ macrocycle phosphopolytungstate, *Inorg. Chem.*, 2019, **58**, 1091–1099.

49 V. S. Korenev, P. A. Abramov, A. L. Gushchin, D. V. Stass, V. M. Babaev, I. K. Rizvanov and M. N. Sokolov, Uranyl

incorporation into the polyoxometalate cavity. Synthesis and characterization of $[(\text{UO}_2)_8\text{P}_8\text{W}_{48}\text{O}_{184}]^{24-}$, *Russ. J. Inorg. Chem.*, 2019, **64**, 1105–1114.

50 J. Goura, A. Sundar, B. S. Bassil, G. Ćirić-Marjanović, D. Bajuk-Bogdanović and U. Kortz, Peroxouranyl-containing W_{48} wheel: synthesis, structure, and detailed infrared and raman spectroscopy study, *Inorg. Chem.*, 2020, **59**, 16789–16794.

51 M. Y. Cheng, Y. F. Liu, W. X. Du, J. W. Shi, J. H. Li, H. Y. Wang, K. Li, G. P. Yang and D. D. Zhang, Two Dawson-type U(vi)-containing selenotungstates with sandwich structure and its high-efficiency catalysis for pyrazoles, *Chin. Chem. Lett.*, 2022, **33**, 3899–3902.

52 V. N. Molchanov, I. V. Tatjanina, E. A. Torchenkova and L. P. Kazansky, A novel type of heteropolyacid complex anion: X-ray crystal structure of the polymeric complex anion $[\text{Th}(\text{H}_2\text{O})_3\text{UMo}_{12}\text{O}_{42}]_n^{4n-}$, *J. Chem. Soc., Chem. Commun.*, 1981, 93–94.

53 M. A. Petrukhina, V. N. Molchanov, I. V. Tat'yanina and E. A. Torchenkova, Crystal structure of heteropolycomplex $[(\text{CH}_3)_4\text{N}]_2[\text{Fe}_2^{3+}(\text{H}_2\text{O})_6\text{UMo}_{12}\text{O}_{42}] \cdot 18\text{H}_2\text{O}$, *Kristallografiya*, 1990, **35**, 386–389.

54 M. A. Petrukhina, V. S. Sergienko, G. G. Sadikov, I. V. Tat'yanina and E. A. Torchenkova, Crystal structure of heteropolycomplex $[(\text{CH}_3)_4\text{N}]_2\text{H}_2[\text{Cu}(\text{H}_2\text{O})_6\text{UMo}_{12}\text{O}_{42}] \cdot n\text{H}_2\text{O}$, *Koord. Khim.*, 1990, **16**, 354–360.

55 E. P. Samokhvalova, V. N. Molchanov, I. V. Tat'yanina and E. A. Torchenkova, Crystal structure of $(\text{NH}_4)_2[\text{Sc}_2\text{UMo}_{12}\text{O}_{42}] \cdot 26\text{H}_2\text{O}$, *Koord. Khim.*, 1990, **16**, 207–211.

56 E. P. Samokhvalova, V. N. Molchanov, I. V. Tat'yanina and E. A. Torchenkova, Crystal structure of $\text{H}_2[\text{Nd}_2(\text{H}_2\text{O})_{12}\text{UMo}_{12}\text{O}_{42}] \cdot 12\text{H}_2\text{O}$, *Koord. Khim.*, 1990, **16**, 1277–1282.

57 I. V. Tat'yanina, E. B. Fomicheva, V. N. Molchanov, V. E. Zavodnik, V. K. Bel'skij and E. A. Torchenkova, Crystal structure of $(\text{NH}_4)_2[\text{Er}_2\text{UMo}_{12}\text{O}_{42}] \cdot x22\text{H}_2\text{O}$, *Kristallografiya*, 1982, **27**, 233–238.

58 M. K. Kotvanova, V. N. Molchanov, E. A. Torchenkova and V. I. Spitsyn, $(\text{NH}_4)_4[\text{UO}_2)_2(\text{OH}_2)_3\text{UMo}_{12}\text{O}_{42}] \cdot 18\text{H}_2\text{O}$ Crystal-structure, *Zh. Neorg. Khim.*, 1984, **29**, 1790–1797.

59 M. K. Kotvanova, V. N. Molchanov, E. A. Torchenkova and K. I. Kim, Crystal structure of $[(\text{C}_2\text{H}_5)_4\text{N}]_4[(\text{VO})_2(\text{OH}_2)_4\text{UMo}_{12}\text{O}_{42}] \cdot x8\text{H}_2\text{O}$, *Koord. Khim.*, 1984, **10**, 993–997.

60 K.-C. Kim and M. T. Pope, New plenary and lacunary polyoxotungstate structures assembled from nonatungstostearate(III) anions and uranyl cations, *J. Chem. Soc., Dalton Trans.*, 2001, 986–990.

61 Y. Jeannin, Synthesis and crystallographic study of a new composite of assymmetric coordination of uranium(iv) linked to two ligands of the polytungstate type $[(\text{H}_3\text{Sb}^{\text{III}}\text{W}_{17}\text{O}_{59})\text{U}^{\text{IV}}(\text{HW}_5\text{O}_{18})]^{11-}$, *C. R. Chim.*, 2005, **8**, 999–1004.

62 M. Y. Cheng, H. Y. Wang, Y. F. Liu, J. W. Shi, M. Q. Zhou, W. X. Du, D. D. Zhang and G. P. Yang, Bouquet-like uranium-containing selenotungstate consisting of two different Keggin-/Anderson-type units with excellent photoluminescence quantum yield, *Chin. Chem. Lett.*, 2022, DOI: [10.1016/j.cclet.2022.02.015](https://doi.org/10.1016/j.cclet.2022.02.015).

63 M. H. Dickman, G. J. Gama, K.-C. Kim and M. T. Pope, The structures of europium(III)- and uranium(IV) derivatives of $[\text{P}_5\text{W}_{30}\text{O}_{110}]^{15-}$: Evidence for “Cryptohydration”, *J. Cluster Sci.*, 1996, **7**, 567–583.

64 M. Dufaye, S. Duval, B. Hirsou, G. Stoclet and T. Loiseau, Complexation of tetravalent uranium cations by the $\text{As}_4\text{W}_{40}\text{O}_{140}$ cryptand, *CrystEngComm*, 2018, **20**, 5500–5509.

65 G. Marcu, M. Rusu and D. Rusu, Homogeneous isotope exchange between tungsten(vi) and Keggin and Dawson type uranium polyoxotungstophosphates, *J. Radioanal. Nucl. Chem.*, 1999, **242**, 119–122.

66 M. Rusu, Spectrophotometric and paper electrophoretic studies of uranium(IV) polyoxotungstogermanate complexes, *J. Radioanal. Nucl. Chem.*, 2000, **245**, 353–356.

67 M. Rusu, D. Rusu, C. Roșu, C. Crăciun, L. David, A.-R. Tomșa and G. Marcu, Keggin polyoxotungstoborate with uranium(IV), *J. Radioanal. Nucl. Chem.*, 2000, **245**, 363–366.

68 C. Crăciun and L. David, Spectroscopic and magnetic investigation of one sandwich-type uranium(IV)-polyoxometalate with Ge(IV) as heteroatom, *J. Alloys Compd.*, 2001, **323**, 743–747.

69 C. Crăciun, L. David, D. Rusu, M. Rusu, O. Cozar and G. Marcu, Complexation of three uranium(IV) ions at two $\alpha\text{-B}[\text{SbW}_3\text{O}_{33}]^{9-}$ trilacunary Keggin units: A spectroscopic investigation, *J. Radioanal. Nucl. Chem.*, 2001, **247**, 307–310.

70 C. Crăciun, D. Rusu, L. Pop-Fanea, M. Hossu, M. Rusu and L. David, Spectroscopic investigation of several uranium(IV) polyoxometalate complexes, *J. Radioanal. Nucl. Chem.*, 2005, **264**, 589–594.

71 M. Rusu, G. Marcu, D. Rusu, C. Roșu and A.-R. Tomșa, Uranium(IV) polyoxotungstophosphates, *J. Radioanal. Nucl. Chem.*, 1999, **242**, 467–472.

72 I. Creaser, M. C. Heckel, R. J. Neitz and M. T. Pope, Rigid nonlabile polyoxometalate cryptates $[\text{ZP}_5\text{W}_{30}\text{O}_{110}]^{(15-n)-}$ that exhibit unprecedented selectivity for certain lanthanide and other multivalent cations, *Inorg. Chem.*, 1993, **32**, 1573–1578.

73 H. F. Li, W. J. Chen, Y. J. Zhao, Y. Zou, X. Zhao, J. P. Song, P. T. Ma, J. Y. Niu and J. P. Wang, Regulating the catalytic activity of multi-Ru-bridged polyoxometalates based on differential active site environments with six-coordinate geometry and five-coordinate geometry transitions, *Nanoscale*, 2021, **13**, 8077–8086.

74 M. Nyman and P. C. Burns, A comprehensive comparison of transition-metal and actinyl polyoxometalates, *Chem. Soc. Rev.*, 2012, **41**, 7354–7367.

75 P. C. Burns, Nanoscale uranium-based cage clusters inspired by uranium mineralogy, *Mineral. Mag.*, 2011, **75**, 1–25.

76 P. C. Burns and M. Nyman, Captivation with encapsulation: a dozen years of exploring uranyl peroxide capsules, *Dalton Trans.*, 2018, **47**, 5916–5927.

77 S. Hickam, J. Breier, Y. Cripe, E. Cole and P. C. Burns, Effects of H_2O_2 concentration on formation of uranyl peroxide species probed by dissolution of uranium nitride and uranium dioxide, *Inorg. Chem.*, 2019, **58**, 5858–5864.

78 L. Zhang, M. Dembowski, A. Arteaga, S. Hickam, N. P. Martin, L. N. Zakharov, M. Nyman and P. C. Burns, Energetic trends in monomer building blocks for uranyl peroxide clusters, *Inorg. Chem.*, 2019, **58**, 439–445.

79 A. Arteaga, D. Ray, E. N. Glass, N. P. Martin, L. N. Zakharov, L. Gagliardi and M. Nyman, The role of the organic solvent polarity in isolating uranyl peroxide capsule fragments, *Inorg. Chem.*, 2020, **59**, 1633–1641.

80 A. V. Virovets, E. Peresypkina and M. Scheer, Structural chemistry of giant metal based supramolecules, *Chem. Rev.*, 2021, **121**, 14485–14554.

81 W. T. Yang, T. G. Parker and Z. M. Sun, Structural chemistry of uranium phosphonates, *Coord. Chem. Rev.*, 2015, **303**, 86–109.

82 G. E. Sigmon, B. Weaver, K.-A. Kubatko and P. C. Burns, Crown and bowl-shaped clusters of uranyl polyhedra, *Inorg. Chem.*, 2009, **48**, 10907–10909.

83 Z. L. Liao, J. Ling, L. R. Reinke, J. E. S. Szymanowski, G. E. Sigmon and P. C. Burns, Cage clusters built from uranyl ions bridged through peroxy and 1-hydroxyethane-1,1-diphosphonic acid ligands, *Dalton Trans.*, 2013, **42**, 6793–6802.

84 J. Ling, J. Qiu, G. E. Sigmon, M. Ward, J. E. S. Szymanowski and P. C. Burns, Uranium pyrophosphate/methylenediphosphonate polyoxometalate cage clusters, *J. Am. Chem. Soc.*, 2010, **132**, 13395–13402.

85 J. Ling, H. X. Zhang, J. Qiu, M. Stoffer, D. Burgess and P. C. Burns, Pyrophosphate and methylenediphosphonate incorporated uranyl peroxide cage clusters, *Cryst. Growth Des.*, 2018, **18**, 7720–7729.

86 M. Y. Xu, H. Traustason, F. D. Bo, S. Hickam, S. Chong, L. Zhang, A. G. Oliver and P. C. Burns, Supramolecular assembly of geometrically unstable hybrid organic–inorganic uranyl peroxide cage clusters and their transformations, *J. Am. Chem. Soc.*, 2019, **141**, 12780–12788.

87 G. E. Sigmon, J. Ling, D. K. Unruh, L. Moore-Shay, M. Ward, B. Weaver and P. C. Burns, Uranyl–peroxide interactions favor nanocluster self-assembly, *J. Am. Chem. Soc.*, 2009, **131**, 16648–16649.

88 J. Qiu, T. L. Spano, M. Dembowski, A. M. Kokot, J. E. S. Szymanowski and P. C. Burns, Sulfate-centered sodium-icosahedron-templated uranyl peroxide phosphate cages with uranyl bridged by $\mu\text{-}\eta^1,\text{:}\eta^2$ peroxide, *Inorg. Chem.*, 2017, **56**, 1874–1880.

89 M. Y. Xu, P. Eckard and P. C. Burns, Organic functionalization of uranyl peroxide clusters to impact solubility, *Inorg. Chem.*, 2020, **59**, 9881–9888.

90 J. Qiu, K. Nguyen, L. Jouffret, J. E. S. Szymanowski and P. C. Burns, Time-resolved assembly of chiral uranyl peroxy cage clusters containing belts of polyhedra, *Inorg. Chem.*, 2013, **52**, 337–345.

91 P. C. Burns, K. A. Kubatko, G. Sigmon, B. J. Fryer, J. E. Gagnon, M. R. Antonio and L. Soderholm, Actinyl peroxide nanospheres, *Angew. Chem., Int. Ed.*, 2005, **44**, 2135–2139.

92 D. K. Unruh, A. Burtner, L. Pressprich, G. E. Sigmon and P. C. Burns, Uranyl peroxide closed clusters containing topological squares, *Dalton Trans.*, 2010, **39**, 5807–5813.

93 D. K. Unruh, J. Ling, J. Qiu, L. Pressprich, M. Baranay, M. Ward and P. C. Burns, Complex nanoscale cage clusters built from uranyl polyhedra and phosphate tetrahedra, *Inorg. Chem.*, 2011, **50**, 5509–5516.

94 J. Ling, M. Ozga, M. Stoffer and P. C. Burns, Uranyl peroxide pyrophosphate cage clusters with oxalate and nitrate bridges, *Dalton Trans.*, 2012, **41**, 7278–7284.

95 G. E. Sigmon and P. C. Burns, Rapid self-assembly of uranyl polyhedra into crown clusters, *J. Am. Chem. Soc.*, 2011, **133**, 9137–9139.

96 G. E. Sigmon, D. K. Unruh, J. Ling, B. Weaver, M. Ward, L. Pressprich, A. Simonetti and P. C. Burns, Symmetry versus minimal pentagonal adjacencies in uranium-based polyoxometalate fullerene topologies, *Angew. Chem., Int. Ed.*, 2009, **48**, 2737–2740.

97 J. Ling, C. M. Wallace, J. E. S. Szymanowski and P. C. Burns, Hybrid uranium–oxalate fullerene topology cage clusters, *Angew. Chem., Int. Ed.*, 2010, **49**, 7271–7273.

98 T. Z. Forbes, J. G. McAlpin, R. Murphy and P. C. Burns, Metal–oxygen isopolyhedra assembled into fullerene topologies, *Angew. Chem., Int. Ed.*, 2008, **47**, 2824–2827.

99 J. Ling, J. Qiu and P. C. Burns, Uranyl peroxide oxalate cage and core–shell clusters containing 50 and 120 uranyl ions, *Inorg. Chem.*, 2012, **51**, 2403–2408.

100 J. Qiu, J. Ling, A. Sui, J. E. S. Szymanowski, A. Simonetti and P. C. Burns, Time-resolved self-assembly of a fullerene-topology core–shell cluster containing 68 uranyl polyhedra, *J. Am. Chem. Soc.*, 2012, **134**, 1810–1816.

101 J. Qiu, J. Ling, L. Jouffret, R. Thomas, J. E. S. Szymanowski and P. C. Burns, Water-soluble multi-cage super tetrahedral uranyl peroxide phosphate clusters, *Chem. Sci.*, 2014, **5**, 303–310.

102 M. Dembowski, C. D. Pilgrim, S. Hickam, T. L. Spano, D. Hamlin, A. G. Oliver, W. H. Casey and P. C. Burns, Dynamics of cation-induced conformational changes in nanometer-sized uranyl peroxide clusters, *Inorg. Chem.*, 2020, **59**, 2495–2502.

103 O. Renier, C. Falaise, H. Neal, K. Kozma and M. Nyman, Closing uranyl polyoxometalate capsules with bismuth and lead polyoxocations, *Angew. Chem., Int. Ed.*, 2016, **55**, 13480–13484.

104 M. Nyman, M. A. Rodriguez and T. M. Alam, The U_{28} nanosphere: what's inside?, *Eur. J. Inorg. Chem.*, 2011, **2011**, 2197–2205.

105 M. Sharifironizi, J. E. S. Szymanowski, J. Qiu, S. Castillo, S. Hickam and P. C. Burns, Charge density influence on enthalpy of formation of uranyl peroxide cage cluster salts, *Inorg. Chem.*, 2018, **57**, 11456–11462.

106 H. Traustason, H. L. Lobeck, P. A. Julien, M. Y. Xu, M. Dembowski and P. C. Burns, Prediction of solution behavior via calorimetric measurements allows for detailed elucidation of polyoxometalate transformation, *Inorg. Chem.*, 2021, **60**, 6753–6763.

107 H. L. Lobeck, J. K. Isner and P. C. Burns, Transformation of uranyl peroxide studtite, $[(\text{UO}_2)(\text{O}_2)(\text{H}_2\text{O})_2](\text{H}_2\text{O})_2$, to soluble nanoscale cage clusters, *Inorg. Chem.*, 2019, **58**, 6781–6789.

108 A. Arteaga, L. Zhang, S. Hickam, M. Dembowski, P. C. Burns and M. Nyman, Uranyl peroxide capsule self-assembly in slow motion, *Chem. – Eur. J.*, 2019, **25**, 6087–6091.

109 D. V. Kravchuk and T. Z. Forbes, In situ generation of organic peroxide to create a nanotubular uranyl peroxide phosphate, *Angew. Chem., Int. Ed.*, 2019, **58**, 18429–18433.

110 M. Fairley, D. E. Felton, G. E. Sigmon, J. E. S. Szymanski, N. A. Poole, M. Nyman, P. C. Burns and J. A. LaVerne, Radiation-induced solid-state transformations of uranyl peroxides, *Inorg. Chem.*, 2022, **61**, 882–889.

111 D. E. Felton, M. Fairley, A. Arteaga, M. Nyman, J. A. LaVerne and P. C. Burns, Gamma-ray-induced formation of uranyl peroxide cage clusters, *Inorg. Chem.*, 2022, **61**, 11916–11922.

112 J. Ling, F. Hobbs, S. Prendergast, P. O. Adelani, J. M. Babo, J. Qiu, Z. H. Weng and P. C. Burns, Hybrid uranium–transition-metal oxide cage clusters, *Inorg. Chem.*, 2014, **53**, 12877–12884.

113 G. A. Senchyk, E. M. Wylie, S. Prizio, J. E. S. Szymanski, G. E. Sigmon and P. C. Burns, Hybrid uranyl–vanadium nano-wheels, *Chem. Commun.*, 2015, **51**, 10134–10137.

114 J. Qiu, M. Dembowski, J. E. S. Szymanski, W. C. Toh and P. C. Burns, Time-resolved X-ray scattering and Raman spectroscopic studies of formation of a uranium–vanadium–phosphorus–peroxide cage cluster, *Inorg. Chem.*, 2016, **55**, 7061–7067.

115 J. Qiu, S. N. Dong, J. E. S. Szymanski, M. Dobrowolska and P. C. Burns, Uranyl–peroxide clusters incorporating iron trimers and bridging by bisphosphonate-and carboxylate-containing ligands, *Inorg. Chem.*, 2017, **56**, 3738–3741.

116 I. Colliard, G. Morrison, H.-C. Z. Loyer and M. Nyman, Supramolecular assembly of U(IV) clusters and superatoms with unconventional counterions, *J. Am. Chem. Soc.*, 2020, **142**, 9039–9047.

117 I. Colliard and M. Nyman, Building $[\text{U}^{\text{IV}70}(\text{OH})_{36}(\text{O})_{64}]^{4-}$ oxocluster frameworks with sulfate, transition metals, and UV, *Chem. – Eur. J.*, 2020, **26**, 12481–12488.

118 T. A. Kohlgruber, G. A. Senchyk, V. G. Rodriguez, S. A. Mackley, F. Dal Bo, S. M. Aksanov, J. E. S. Szymanski, G. E. Sigmon, A. G. Oliver and P. C. Burns, Ionothermal synthesis of uranyl vanadate nanoshell heteropolyoxometalates, *Inorg. Chem.*, 2021, **60**, 3355–3364.

119 J.-C. Berthet, P. Thuéry and M. Ephritikhine, Unprecedented reduction of the uranyl ion $[\text{UO}_2]^{2+}$ into a polyoxo uranium(IV) cluster: Synthesis and crystal structure of the first f-element oxide with a $\text{M}_6(\mu_3\text{-O})_8$ core, *Chem. Commun.*, 2005, 3415–3417.

120 G. Nocton, J. Pécaut, Y. Filinchuk and M. Mazzanti, Ligand assisted cleavage of uranium oxo-clusters, *Chem. Commun.*, 2010, **46**, 2757–2759.

121 N. P. Martin, J. März, C. Volkinger, N. Henry, C. Hennig, A. Ikeda-Ohno and T. Loiseau, Synthesis of coordination polymers of tetravalent actinides (uranium and neptunium) with a phthalate or mellitate ligand in an aqueous medium, *Inorg. Chem.*, 2017, **56**, 2902–2913.

122 D. D. Liu, Y. L. Wang, F. Luo and Q. Y. Liu, Rare three-dimensional uranyl–biphenyl-3,3'-disulfonyl-4,4'-dicarboxylate frameworks: Crystal structures, proton conductivity, and luminescence, *Inorg. Chem.*, 2020, **59**, 2952–2960.

123 D. X. Gu, W. T. Yang, H. P. Chen, Y. H. Yang, X. D. Qin, L. Chen, S. A. Wang and Q. H. Pan, A stable mixed-valent uranium (V,VI) organic framework as a fluorescence thermometer, *Inorg. Chem. Front.*, 2021, **8**, 3514–3521.

124 N. Kumar, R. Bhowal, D. Chopra and A. K. Paul, Structural enhancement under X-ray irradiation in an octanuclear uranium-based 3D metal–organic framework, *Cryst. Growth Des.*, 2021, **21**, 5503–5507.

125 M. Dufaye, N. P. Martin, S. Duval, C. Volkinger, A. Ikeda-Ohno and T. Loiseau, Time-controlled synthesis of the 3D coordination polymer $\text{U}(1,2,3\text{-Hbtc})_2$ followed by the formation of molecular poly-oxo cluster $\{\text{U}_{14}\}$ containing hemimellitate uranium(IV), *RSC Adv.*, 2019, **9**, 22795–22804.

126 K. Lv, S. Fichter, M. Gu, J. März and M. Schmidt, An updated status and trends in actinide metal–organic frameworks (An-MOFs): From synthesis to application, *Coord. Chem. Rev.*, 2021, **446**, 214011.

127 L. Salmon, P. Thuéry and M. Ephritikhine, Crystal structure of the first octanuclear uranium(IV) complex with compartmental Schiff base ligands, *Polyhedron*, 2004, **23**, 623–627.

128 L. Chatelain, S. White, R. Scopelliti and M. Mazzanti, Isolation of a star-shaped uranium(V,VI) cluster from the anaerobic photochemical reduction of uranyl(IV), *Angew. Chem., Int. Ed.*, 2016, **55**, 14325–14329.

129 B. Biswas, V. Mougel, J. Pécaut and M. Mazzanti, Base-driven assembly of large uranium oxo/hydroxo clusters, *Angew. Chem., Int. Ed.*, 2011, **50**, 5745–5748.

130 N. A. Vanagas, J. N. Wacker, C. L. Rom, E. N. Glass, I. Colliard, Y. S. Qiao, J. A. Bertke, E. Van Keuren, E. J. Schelter, M. Nyman and K. E. Knope, Solution and solid state structural chemistry of Th(IV) and U(IV) 4-hydroxybenzoates, *Inorg. Chem.*, 2018, **57**, 7259–7269.

131 Z. H. Yue, X. F. Guo, M. L. Feng, Y. J. Lin, Y. Ju, X. Lin, Z. H. Zhang, X. J. Guo, J. Lin and Y. Y. Huang, Unexpected roles of alkali-metal cations in the assembly of low-valent uranium sulfate molecular complexes, *Inorg. Chem.*, 2020, **59**, 2348–2357.

132 I. Colliard, C. Falaise and M. Nyman, Bridging the transuranics with uranium(IV) sulfate aqueous species and solid phases, *Inorg. Chem.*, 2020, **59**, 17049–17057.

133 N. A. Vanagas, R. F. Higgins, J. N. Wacker, D. R. C. Asuigui, E. Warzecha, S. A. Kozimor, S. L. Stoll, E. J. Schelter, J. A. Bertke and K. E. Knope, Mononuclear to polynuclear U(IV) structural units: effects of reaction conditions on U-furoate phase formation, *Chem. – Eur. J.*, 2020, **26**, 5872–5886.

134 C. Falaise, C. Volkrieger, J.-F. Vigier, A. Beaurain, P. Roussel, P. Rabu and T. Loiseau, Isolation of the large {actinide}₃₈ poly-oxo cluster with uranium, *J. Am. Chem. Soc.*, 2013, **135**, 15678–15681.

135 N. P. Martin, C. Volkrieger, N. Henry, X. Trivelli, G. Stoclet, A. Ikeda-Ohno and T. Loiseau, Formation of a new type of uranium(IV) poly-oxo cluster {U₃₈} based on a controlled release of water via esterification reaction, *Chem. Sci.*, 2018, **9**, 5021–5032.

136 L. Chatelain, R. Faizova, F. Fadaei-Tirani, J. Pécaut and M. Mazzanti, Structural snapshots of cluster growth from {U₆} to {U₃₈} during the hydrolysis of UCl₄, *Angew. Chem., Int. Ed.*, 2019, **58**, 3021–3026.

137 C. Falaise, C. Volkrieger, C. Hennig and T. Loiseau, Ex-situ kinetic investigations of the formation of the poly-oxo cluster U₃₈, *Chem. – Eur. J.*, 2015, **21**, 16654–16664.

138 S. Fichter, T. Radoske and A. Ikeda-Ohno, Structure of the {U₁₃} polyoxo cluster U₁₃O₈Cl_x(MeO)^{38-x} (x=2.3, MeO=methoxide), *Acta Crystallogr., Sect. E: Crystallogr. Commun.*, 2021, **77**, 847–852.

139 M. X. Zhang, C. Y. Liang, G. D. Cheng, J. C. Chen, Y. M. Wang, L. W. He, L. W. Cheng, S. C. Gong, D. Zhang, J. Li, S. X. Hu, J. Diwu, G. Z. Wu, Y. X. Wang, Z. F. Chai and S. A. Wang, Intrinsic semiconducting behavior in a large mixed-valent uranium(V/VI) cluster, *Angew. Chem., Int. Ed.*, 2021, **60**, 9886–9890.

140 V. W. Day, C. W. Earley, W. G. Klemperer and D. J. Maltbie, Synthesis, structure, and reactivity of the {[(η₅-C₅H₅)₂U]2[2(μ,-κ²O-TiW₅O₁₉)₂]}⁴⁻ anion, *J. Am. Chem. Soc.*, 1985, **107**, 8261–8262.

141 P. B. Duval, C. J. Burns, D. L. Clark, D. E. Morris, B. L. Scott, J. D. Thompson, E. L. Werkema, L. Jia and R. A. Andersen, Synthesis and structural characterization of the first uranium cluster containing an isopolyoxometalate core, *Angew. Chem., Int. Ed.*, 2001, **40**, 3357–3361.

142 P. Miró, J. Ling, J. Qiu, P. C. Burns, L. Gagliardi and C. J. Cramer, Experimental and computational study of a new wheel-shaped {[W₅O₂₁]₃[(U^{VI}O₂)₂(μ-O₂)₃]}³⁰⁻ polyoxometalate, *Inorg. Chem.*, 2012, **51**, 8784–8790.

143 T. Deb, L. Zakharov, C. Falaise and M. Nyman, Structure and solution speciation of U^{IV} linked phosphomolybdate (Mo^V) clusters, *Inorg. Chem.*, 2016, **55**, 755–761.

144 N. P. Martin, E. Petrus, M. Segado, A. Arteaga, L. N. Zakharov, C. Bo and M. Nyman, Strategic capture of the {Nb₇} polyoxometalate, *Chem. – Eur. J.*, 2019, **25**, 10580–10584.

145 Y. J. Zhang, T. Wei, T. T. Tran, K. T. Lu, Z. M. Zhang, J. R. Price, I. Aharonovich and R. Zheng, {[U(H₂O)₂]}₂[(UO₂)₁₀O₁₀(OH)₂][(UO₄)(H₂O)₂]}: A mixed-valence uranium oxide hydrate framework, *Inorg. Chem.*, 2020, **59**, 12166–12175.

146 S. C. Termes and M. T. Pope, Stabilization of uranium(IV) in heteropoly anions, *Transition Met. Chem.*, 1978, **3**, 103–108.

147 M. Nyman, Small-angle X-ray scattering to determine solution speciation of metal-oxo clusters, *Coord. Chem. Rev.*, 2017, **352**, 461–472.

148 H. A. Neal, J. Szymanowski, J. B. Fein, P. C. Burns and M. Nyman, Benchmarking uranyl peroxide capsule chemistry in organic media, *Eur. J. Inorg. Chem.*, 2017, **2017**, 39–46.

149 M. Dembowski, T. A. Olds, K. L. Pellegrini, C. Hoffmann, X. P. Wang, S. Hickam, J. H. He, A. G. Oliver and P. C. Burns, Solution ³¹P NMR study of the acid-catalyzed formation of a highly charged {U₂₄P₁₂} nanocluster, {[UO₂)₂₄(O₂)₂₄(P₂O₇)₁₂]¹⁸⁻, and its structural characterization in the solid state using single-crystal neutron diffraction, *J. Am. Chem. Soc.*, 2016, **138**, 8547–8553.

150 T. A. Olds, M. Dembowski, X. P. Wang, C. Hoffman, T. M. Alam, S. Hickam, K. L. Pellegrini, J. H. He and P. C. Burns, Single-crystal time-of-flight neutron diffraction and magic-angle-spinning NMR spectroscopy resolve the structure and 1H and 7Li dynamics of the uranyl peroxide nanocluster U₆₀, *Inorg. Chem.*, 2017, **56**, 9676–9683.

151 S. Hickam, S. M. Aksenen, M. Dembowski, S. N. Perry, H. Traustason, M. Russell and P. C. Burns, Complexity of uranyl peroxide cluster speciation from alkali-directed oxidative dissolution of uranium dioxide, *Inorg. Chem.*, 2018, **57**, 9296–9305.

152 P. Miró, B. Vlaisavljevich, A. Gil, P. C. Burns, M. Nyman and C. Bo, Self-assembly of uranyl-peroxide nanocapsules in basic peroxidic environments, *Chem. – Eur. J.*, 2016, **22**, 8571–8578.

153 J. A. Soltis, C. M. Wallace, R. L. Penn and P. C. Burns, Cation-dependent hierarchical assembly of U₆₀ nanoclusters into macro-ion assemblies imaged via cryogenic transmission electron microscopy, *J. Am. Chem. Soc.*, 2016, **138**, 191–198.

154 D. Li, S. Simotwo, M. Nyman and T. B. Liu, Evolution of actinyl peroxide clusters U₂₈ in dilute electrolyte solution: exploring the transition from simple ions to macroionic assemblies, *Chem. – Eur. J.*, 2014, **20**, 1683–1690.

155 Y. Y. Gao, F. Haso, J. E. S. Szymanowski, J. Zhou, L. Hu, P. C. Burns and T. B. Liu, Selective permeability of uranyl peroxide nanocages to different alkali ions: influences from surface pores and hydration shells, *Chem. – Eur. J.*, 2015, **21**, 18785–18790.

156 A. B. Yusov, V. P. Shilov and A. M. Fedoseev, Stability of actinide (III, IV) and lanthanide (III, IV) complexes with P₂W₁₇O₆₁¹⁰⁻ heteropolyanions, *Radiochemistry*, 2007, **49**, 135–143.

157 G. R. Choppin, Complexation of 4f and 5f cations with polyoxometalates, *J. Nucl. Sci. Technol.*, 2002, **39**, 229–232.

158 K. Wassermann, M. T. Pope, M. Salmen, J. N. Dann and H.-J. Lunk, Thermal degradation of polyoxotungstates-an

effective method for the preparation of tungsten bronzes, *J. Solid State Chem.*, 2000, **149**, 378–383.

159 L. R. Sadergaski, M. Said and A. E. Hixon, Calcium-facilitated aggregation and precipitation of the uranyl peroxide nanocluster U_{60} in the presence of Na-montmorillonite, *Environ. Sci. Technol.*, 2019, **53**, 4922–4930.

160 L. R. Sadergaski and A. E. Hixon, Kinetics of uranyl peroxide nanocluster (U_{60}) sorption to goethite, *Environ. Sci. Technol.*, 2018, **52**, 9818–9826.

161 E. M. Wylie, K. M. Peruski, J. L. Weidman, W. A. Phillip and P. C. Burns, Ultrafiltration of uranyl peroxide nanoclusters for the separation of uranium from aqueous solution, *ACS Appl. Mater. Interfaces*, 2014, **6**, 473–479.

162 C. R. Armstrong, M. Nyman, T. Shvareva, G. E. Sigmon, P. C. Burns and A. Navrotsky, Uranyl peroxide enhanced nuclear fuel corrosion in seawater, *Proc. Natl. Acad. Sci. U. S. A.*, 2012, **109**, 1874–1877.

163 F. Blanchard, M. Ellart, M. Rivenet, N. Vigier, I. Hablot, B. Morel, S. Grandjean and F. Abraham, Neodymium uranyl peroxide synthesis by ion exchange on ammonium uranyl peroxide nanoclusters, *Chem. Commun.*, 2016, **52**, 3947–3950.

164 J. Hu, L. K. Cai, H. H. Wang, K. Chen and P. C. Yin, Uranyl peroxide nanocage assemblies for solid-state electrolytes, *ACS Appl. Nano Mater.*, 2021, **4**, 3597–3603.